

Estimating entanglement in 2D Heisenberg model in the strong rung-coupling limit

Chandrima B. Pushpan, Harikrishnan K. J., Prithvi Narayan, Amit Kumar Pal
Department of Physics, Indian Institute of Technology Palakkad, Palakkad 678 623, India
(Dated: January 12, 2023)

In this paper, we calculate entanglement in the isotropic Heisenberg model in a magnetic field on a two-dimensional rectangular zig-zag lattice in the strong rung-coupling limit, using the one-dimensional XXZ model as a proxy. Focusing on the leading order in perturbation, for arbitrary size of the lattice, we show how the one-dimensional effective description emerges. We point out specific states in the low-energy sector of the two-dimensional model that are well-approximated by the one-dimensional spin-1/2 XXZ model. We propose a systematic approach for mapping matrix-elements of operators defined on the two-dimensional model to their low-energy counterparts on the one-dimensional XXZ model. We also show that partial trace-based description of entanglement in the two-dimensional model can be satisfactorily approximated using the one-dimensional XXZ model as a substitute. We further show numerically that the one-dimensional XXZ model performs well in estimating entanglement quantified using a measurement-based approach in the two-dimensional model for specific choices of measured Hermitian operators.

I. INTRODUCTION

The interface of quantum information theory [1, 2] and *low-dimensional* interacting quantum spin systems [3, 4], with small lattice dimension with each lattice site hosting a Hilbert space of a few levels, has grown into a rich area of interdisciplinary research [5–10] in the past two decades. On one hand, these interacting quantum spin models have been identified as the natural candidates for testing and implementing quantum information and computation protocols, such as quantum state transfer [11–16], measurement-based quantum computation [17–20], and topological quantum error corrections [21–24]. The motivation behind these studies has its origin in the natural occurrence of quantum states with rich quantum correlations belonging to both entanglement-separability [25, 26] and quantum information theoretic paradigms [7], which, alongside being fundamentally important can be used as resource in several quantum tasks [7, 25]. On the other hand, these quantum correlations have provided a refreshing perspective of characterizing quantum many-body systems [5], along with the development of tools and techniques like projected entangled pair states [27–31], and multiscale entanglement renormalization ansatz [32–38]. Current experimental advances allowing implementation and manipulation of these quantum spin models as well as quantum protocols designed on these models using trapped ions [39–43], superconducting qubits [44, 45], nuclear magnetic resonance [46, 47], solid-state systems [48, 49], and ultra-cold atoms [50–54] have also provided a major boost to these studies.

Among a plethora of low-dimensional quantum spin models, two-dimensional (2D) lattice models have always been specially challenging due to the faster growth of Hilbert space dimension with increasing number of spins in the system, compared to their one-dimensional (1D) counterparts. One such model is the Heisenberg model [55–63] in a magnetic field on a rectangular lattice of NL sites, having respectively N and L lattice sites in the horizontal and vertical directions, where each lattice site hosts a spin-1/2 particle. A number of recent studies [64–67] have been carried out to understand the entanglement properties of the model.

Particular attention has been drawn towards quasi-1D models [68, 69] like quantum spin ladders [70–73] with number of lattice sites in the horizontal direction being far greater than the same in the vertical direction ($N \gg L$). As natural extensions of the 1D models while going towards 2D, quantum spin ladders with $L = 2$ has been investigated from the perspective of quantum state transfer [74, 75]. Moreover, entanglement [75–83] and fidelity [79, 84] have been investigated in these ladder models from the perspective of phases characterizations. While most of these studies have concentrated on models with spin-1/2 particles, entanglement properties of quantum spin ladders with higher spin quantum numbers [85] have also been explored.

In the limit where the coupling strength J_{\perp} along the rungs of the ladder are much larger compared to other spin-exchange interactions present in the system, the rung behaves like a single degree of freedom, and the model becomes effectively 1D. By further tuning magnetic field strength, for low values of L ($L = 2, 3$), [86–91] show that the isotropic Heisenberg quantum spin-1/2 ladders map to an 1D XXZ model [92–95]. This mapping has been used to study quantum phase transitions in the case of antiferromagnetic spin-1/2 ladders with $L = 2$ [87–91, 96] and 3 [86, 91], using magnetization properties [87, 88, 90, 91], and entanglement [96] (see also [97] for the mapping in the case of a mixed-spin variant of quantum spin ladders with $L = 2$). While most of these studies have focused on local observables, non-local correlations such as entanglement in the low-energy sector of the spin-1/2 Heisenberg model on a quasi-1D, or 2D lattice, using the effective 1D model as a proxy, is yet to be explored, to the best of our knowledge.

In this paper, we specifically ask *whether entanglement properties in the 1D effective model can approximate the corresponding entanglement in all states of the low-energy manifold of the isotropic Heisenberg model in a magnetic field, defined on a quasi-1D, or 2D rectangular zig-zag lattice (see Fig. 1(a)).* Towards approaching this question, we lay the ground by determining the 1D effective model in a system size-independent fashion, thereby bringing the specific models, studied so far in a case-by-case basis [86–91, 96], under the same umbrella. As mentioned above, we particularly focus on tuning the magnetic field such that the ground-state

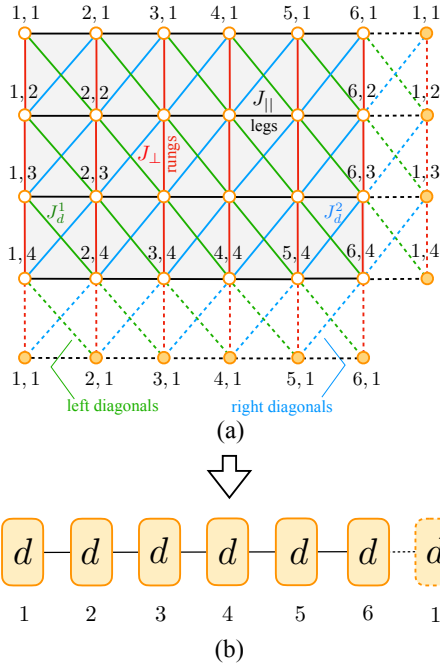


FIG. 1. (a) A two-dimensional zig-zag lattice of 6 rungs and 4 legs holding 6×4 spin- $\frac{1}{2}$ particles. The spin-exchange interaction strength along the rungs and the legs are J_{\perp} and J_{\parallel} , respectively, while the spins interact diagonally with the interaction strengths J_d^1 and J_d^2 along the left and the right diagonals respectively. The periodic boundary condition along the rungs, legs, and diagonals are represented by the dashed links to the edge spins of the lattice. Each spin in the lattice is subjected to a magnetic field of strength h in the z -direction. (b) Using degenerate perturbation theory in the low-energy subspace in the strong rung-coupling limit ($J_{\perp} \gg J_{\parallel}, J_d^1, J_d^2$), for specific points in the parameter space of J_{\perp} and h , the model can be mapped to a effective 1D Hamiltonian (see Eq. (12)), where each lattice site hosts a d -dimensional Hilbert space corresponding to each rung of the system.

degeneracy of the model in the strong rung-coupling limit is two-fold. We prove that the 1D effective Hamiltonian is rotationally invariant about the z -axis to any order in perturbation theory. We focus on the leading order in perturbation, which turns out to be an 1D spin-1/2 XXZ model, which can be dealt with relatively easily due to the computational advantage obtained from the reduction in the Hilbert space, and considerable information is available about the model in literature [92–95]. We analytically derive the effective coupling constants of the 1D XXZ model as functions of the coupling constants in the original model for arbitrary values of N and L and for different boundary conditions on the 2D lattice in the horizontal and vertical directions. We also point out a set of typical states including the thermal state and the time-evolved state constituted from the low-energy sector of the model for which the effective 1D theory works, up to $\mathcal{O}(J_{\perp}^{-1})$, in estimating the states. We give a systematic prescription for mapping matrix-elements of operators among these states to their 1d effective counterparts. We also show that the entanglement in low-energy states of the quasi-1D or 2D model is satisfactorily proxied by the entanglement

in the corresponding mapped state in the 1D model. We illustrate these results using typical observables and entanglement measures computed using partial trace-based methods. We also investigate measurement-based entanglement in the quasi-1D and 2D model, for which analytical treatment is difficult. However, for certain choices of measured Hermitian operators, our numerical analysis shows that the 1D effective XXZ model can mimic the results in the quasi-1D or 2D model.

The rest of the paper is organized as follows. In Sec. II, we discuss the 2D Heisenberg model, the low-energy 1D effective Hamiltonian, and its symmetry, and point out typical states where the 1D effective theory performs satisfactorily. The technical details of working out the 1D effective XXZ model are included in Sec. III. Sec. IV deals with the performance of the 1D effective theory in computing matrix elements of Hermitian operators, while the application of the 1D effective theory in quantifying entanglement using partial trace-based and measurement-based approaches are included in Sec. V. Sec. VI contains the concluding remarks and outlook.

II. LOW-ENERGY EFFECTIVE HAMILTONIAN

In this section, we introduce the Isotropic Heisenberg model on the rectangular zig-zag lattice, and discuss mapping it to an effective one-dimensional (1D) lattice model in the low-energy subspace.

A. Isotropic Heisenberg model on a 2D zig-zag lattice

Let us consider an $N \times L$ lattice with L (N) lattice sites along the vertical (horizontal) direction, each lattice site hosting a spin- $\frac{1}{2}$ particle (see Fig. 1(a)), such that a 2^{NL} -dimensional Hilbert space \mathcal{H} is associated to the system. We call the vertical (horizontal) lines in the lattice as the *rungs* (*legs*), where N (L) represents the number of rungs (*legs*). While $N = L$ represents a zig-zag square lattice, $N \gg L$ represents a zig-zag *ladder* that is intermediate between the one- and two-dimensional lattices, and is therefore called a *quasi-1D* lattice model [73]. Isotropic Heisenberg interactions [92–95] are present between the spins along the legs, rungs, as well as the diagonals, and an external magnetic field applies to all spins along the z direction. The spin system is represented by the Hamiltonian [73]

$$H/J_{\perp} = H_R + H_I, \quad (1)$$

with

$$H_R = \frac{1}{4} \sum_{i=1}^N \sum_{j=1}^L \vec{\sigma}_{i,j} \cdot \vec{\sigma}_{i,j+1} - \frac{h}{2J_{\perp}} \sum_{i=1}^N \sum_{j=1}^L \sigma_{i,j}^z - NE_g, \quad (2)$$

and

$$H_I = \frac{J_{||}}{4J_{\perp}} \sum_{i=1}^N \sum_{j=1}^L \vec{\sigma}_{i,j} \cdot \vec{\sigma}_{i+1,j} + \frac{J_d^1}{4J_{\perp}} \sum_{i=1}^N \sum_{j=1}^L \vec{\sigma}_{i,j+1} \cdot \vec{\sigma}_{i+1,j} + \frac{J_d^2}{4J_{\perp}} \sum_{i=1}^N \sum_{j=1}^L \vec{\sigma}_{i,j} \cdot \vec{\sigma}_{i+1,j+1}. \quad (3)$$

Here, J_{\perp} ($J_{||}$) is the strength of the spin-exchange interactions along the rungs (along the legs), J_d^1 and J_d^2 are the diagonal interaction strengths, h is the strength of the magnetic field, $\vec{\sigma}_{i,j} \equiv \{\sigma_{i,j}^x, \sigma_{i,j}^y, \sigma_{i,j}^z\}$ are the Pauli operators on the lattice-site denoted by the subscripts i, j , with i (j) being the rung (leg) index running from 1 to N (L), and E_g is a constant we will choose in section II B. We use the computational basis $\{|0\rangle, |1\rangle\}$ to write the Pauli matrices, where $\sigma^z |0\rangle = |0\rangle$, $\sigma^z |1\rangle = -|1\rangle$, such that $|0\rangle \equiv |\uparrow\rangle$, and $|1\rangle \equiv |\downarrow\rangle$.

B. Effective Hamiltonian in low-energy subspace

We now discuss the construction of a low-energy effective 1D Hamiltonian (LEH) [98] corresponding to the spin models described in Sec. II A. We start with the limit $J_{||} = J_d^1 = J_d^2 = 0$, where the model consists of N non-interacting rungs, each of which corresponds to a 2^L -dimensional Hilbert space. The antiferromagnetic isotropic Heisenberg Hamiltonian of each rung is given by

$$H_{R_i} = \frac{1}{4} \sum_{j=1}^L \vec{\sigma}_{i,j} \cdot \vec{\sigma}_{i,j+1} - \frac{h}{2J_{\perp}} \sum_{j=1}^L \sigma_{i,j}^z - E_g, \quad (4)$$

with $H_R = \sum_{i=1}^N H_{R_i}$. Let us assume that for a given value of h , the spectrum of H_{R_i} is given by $\{E_{k_i}^{(i)}, |\psi_{k_i}^{(i)}\rangle\}$, where $k_i \in \{0, 1, \dots, 2^L - 1\} \forall i \in \{1, 2, \dots, N\}$, such that

$$H_{R_i} |\psi_{k_i}^{(i)}\rangle = E_{k_i}^{(i)} |\psi_{k_i}^{(i)}\rangle, \quad (5)$$

with $k_i = 0$ representing the ground state. A d -fold degeneracy in the ground states can be imposed via tuning h to specific values, denoted by h' where typically $h' \sim J_{\perp}$. At this point, we choose E_g such that ground state energy of H_{R_i} with $h = h'$ vanishes. For a fixed L , there may be multiple values of h' resulting in a d -fold degenerate ground state. For each h' , we relabel the states $\{|\psi_{k_i}^{(i)}\rangle\}$ such that

$$E_{k_i}^{(i)} = 0 \forall k_i = 0, 1, 2, \dots, d-1, \\ E_{k_i}^{(i)} > 0 \forall k_i = d, d+2, \dots, 2^L - 1, \quad (6)$$

and denote the d -fold degenerate ground states by $\{|\psi_0^{(i)}\rangle, \dots, |\psi_{d-1}^{(i)}\rangle\}$. For each h' , the ground-state manifold $\{|\Psi_l\rangle\}$ of H_R is d^N -fold degenerate, constituting the low-energy subspace $\mathcal{S} \subset \mathcal{H}$, with $|\Psi_l\rangle$ having the form

$$|\Psi_l\rangle = \bigotimes_{i=1}^N |\psi_{k_i}^{(i)}\rangle. \quad (7)$$

Here, $k_i = 0, 1, \dots, d-1$, and $l = 0, 1, 2, \dots, d^N - 1$ labels the ground state manifold¹. We will find it useful to split the Hilbert space into two subspaces, one is spanned by $|\Psi_l\rangle$ (which we will term as *low energy sector*) and the other (which we will term as *high energy sector*) orthogonal to this space. We can also define a projector onto the low energy sector as

$$P_g = \sum_l |\Psi_l\rangle \langle \Psi_l| \quad (8)$$

and the projector on the high energy sector is $P_e \equiv I - P_g$.

Let us now rewrite the system Hamiltonian H (Eq. (1)) as

$$\frac{1}{J_{\perp}} H = H_0 + \frac{1}{J_{\perp}} H', \quad (9)$$

where

$$H_0 = \frac{1}{4} \sum_{i=1}^N \sum_{j=1}^L \vec{\sigma}_{i,j} \cdot \vec{\sigma}_{i,j+1} - \frac{h'}{2J_{\perp}} \sum_{i=1}^N \sum_{j=1}^L \sigma_{i,j}^z - NE_g, \quad (10)$$

which is H_R at $h = h'$, and

$$H' = \frac{J_{||}}{4} \sum_{i=1}^N \sum_{j=1}^L \vec{\sigma}_{i,j} \cdot \vec{\sigma}_{i+1,j} + \frac{J_d^1}{4} \sum_{i=1}^N \sum_{j=1}^L \vec{\sigma}_{i,j+1} \cdot \vec{\sigma}_{i+1,j} + \frac{J_d^2}{4} \sum_{i=1}^N \sum_{j=1}^L \vec{\sigma}_{i,j} \cdot \vec{\sigma}_{i+1,j+1} - \frac{\Delta h}{2} \sum_{i=1}^N \sum_{j=1}^L \sigma_{i,j}^z, \quad (11)$$

with $\Delta h = h - h'$. Clearly, ground states of H_0 have a d^N -fold degeneracy (see Eq. (7)), which is lifted by the perturbation H' . For $\Delta h, J_{||}, J_d^{1,2} \ll J_{\perp}$, this leads to an effective Hamiltonian operating in the low-energy subspace \mathcal{S} , where energy-eigenvalues of the n -th order ($n = 1, 2, \dots$) effective Hamiltonian in \mathcal{S} provides the n -th order energy corrections to the unperturbed states of low energy. In this paper, we focus only on the first-order ($n = 1$) effective Hamiltonians, which can be obtained as

$$\tilde{H} = \sum_{l,l'=0}^{d^N-1} \langle \Psi_l | H' | \Psi_{l'} \rangle | \Psi_l \rangle \langle \Psi_{l'} |. \quad (12)$$

Note here that the first-order effective Hamiltonian (12) represents a system of one lattice dimension with N -sites, where each lattice site has d degrees of freedom.

In this paper, we focus on a subset of cases with $d = 2$ by choosing h' appropriately. The effective degrees of freedom in this case is like a spin half system. The effective Hamiltonian will be built out of operators acting on this low energy spin-1/2 degree of freedom. While we can use the definition (12) to find the effective Hamiltonian, we find it more instructive to work out the symmetries of the system which will then constrain the structure of the effective Hamiltonian.

¹ Note that l can be identified as the decimal equivalent of the string $k_1 k_2 k_3 \dots k_N$ in base d .

The detailed structure of the effective Hamiltonian can be subsequently worked out. We denote the doubly-degenerate ground states of H_{R_i} at $h = h'$ by $|\psi_0^{(i)}\rangle$ and $|\psi_1^{(i)}\rangle$. Since $[Z_i, H_{R_i}] = 0$, with $Z_i = \sum_{j=1}^L \sigma_{i,j}^z$ defined on the rung i ,

$$Z_i |\psi_k^{(i)}\rangle = m_k |\psi_k^{(i)}\rangle, \quad (13)$$

$k = 0, 1$, where m_k are the eigenvalues of Z_i corresponding to the eigenvectors $|\psi_k^{(i)}\rangle$. Note here that Z_i is the generator of the z -rotation on the Hilbert space of the i th rung. We now propose the following.

■ **Proposition 1.** *If $m_0 \neq m_1$, \tilde{H} is z -rotationally invariant.*

Proof. Consider the operator

$$\mathcal{Z} = \sum_{i=1}^N J_i^z, \quad (14)$$

with

$$J_i^z = a + bZ_i, \quad (15)$$

where \mathcal{Z} is a symmetry of the original system-Hamiltonian H , i.e.,

$$[\mathcal{Z}, H_0] = [\mathcal{Z}, H'] = 0, \quad (16)$$

and a and b are real constants that can be chosen according to convenience. Since $m_0 \neq m_1$, we choose $a = (m_1 + m_0)/(m_1 - m_0)$ and $b = 2/(m_0 - m_1)$ such that

$$J_i^z |\psi_0^{(i)}\rangle = |\psi_0^{(i)}\rangle, \quad J_i^z |\psi_1^{(i)}\rangle = -|\psi_1^{(i)}\rangle. \quad (17)$$

Therefore, the action of J_i^z on the rung-subspace spanned by $|\psi_{0(1)}^{(i)}\rangle$ is similar to that of an *effective* Pauli- z operator², which can be defined as

$$\tau_i^z = |\psi_0^{(i)}\rangle \langle \psi_0^{(i)}| - |\psi_1^{(i)}\rangle \langle \psi_1^{(i)}|. \quad (18)$$

Let us further define the operator $\eta^z = \sum_{i=1}^N \tau_i^z$, and note that

$$\eta^z |\Psi_l\rangle = \mathcal{Z} |\Psi_l\rangle = m_l |\Psi_l\rangle, \quad (19)$$

where $m_l = \sum_{i=1}^N (-1)^{k_i}$ (see Eq. (7)). Since $[\eta_z, H'] = 0$, η_z can't change the eigenvalue under H' and hence $\langle \Psi_l | H' | \Psi_{l'} \rangle = 0$ if $m_l \neq m_{l'}$. Since this vanishes for $m_l \neq m_{l'}$, we have

$$\begin{aligned} [\eta^z, \tilde{H}] &= \sum_{l, l'=0}^{2^N-1} (m_l - m_{l'}) |\Psi_l\rangle \langle \Psi_l | H' | \Psi_{l'} \rangle \langle \Psi_{l'} | \\ &= 0, \end{aligned} \quad (20)$$

implying that η^z is a symmetry of the effective 1D Hamiltonian \tilde{H} . \square

² Note that the assumption $m_0 \neq m_1$ is crucial for the J_i^z s to mimic the action of Pauli- z operators

Since the first order effective Hamiltonian is guaranteed to be at most nearest-neighbour in the effective spins, the following corollary can be written.

◇ **Corollary 1.1** *The most general form of z -rotationally invariant \tilde{H} is a nearest-neighbor XXZ model [93] in a magnetic field, given by*

$$\begin{aligned} \tilde{H} &= \sum_{i=1}^N \left[\tilde{J}_{xy} (\tau_i^x \tau_{i+1}^x + \tau_i^y \tau_{i+1}^y) + \tilde{J}_{zz} \tau_i^z \tau_{i+1}^z \right] \\ &+ \tilde{h} \sum_{i=1}^N \tau_i^z + C, \end{aligned} \quad (21)$$

where C is an irrelevant additive constant.

Here, we have defined

$$\begin{aligned} \tau_i^x &= |\psi_0^{(i)}\rangle \langle \psi_1^{(i)}| + |\psi_1^{(i)}\rangle \langle \psi_0^{(i)}|, \\ \tau_i^y &= -i \left[|\psi_0^{(i)}\rangle \langle \psi_1^{(i)}| - |\psi_1^{(i)}\rangle \langle \psi_0^{(i)}| \right] \end{aligned} \quad (22)$$

as the effective Pauli- x and y operators defined on the rung subspace spanned by $|\psi_{0,1}^{(i)}\rangle$ (see Eq. (18)). The coefficients \tilde{J}_{xy} , \tilde{J}_z , and \tilde{h} can be determined as functions of the couplings in the perturbation Hamiltonian H' , namely, $J_{||}$, $J_d^{1,2}$, and Δh . The exact forms of the functions depend on the forms of the doubly-degenerate ground states $|\psi_{0,1}^{(i)}\rangle$, and subsequently on the specific point $h = h'$ where the perturbation calculation is carried out.

Note 1. In the low-energy sector, it is sufficient to consider the effective Hamiltonian (21) as a model for N spin-1/2 particles, where the Pauli matrices on the Hilbert space of the spin-1/2 particle are given by $\tau^{x,y,z}$. In this picture, we relabel $|\psi_{0,1}^{(i)}\rangle$ as

$$|\mathbf{0}_i\rangle = |\psi_0^{(i)}\rangle, \quad |\mathbf{1}_i\rangle = |\psi_1^{(i)}\rangle, \quad (23)$$

where $\{|\mathbf{0}_i\rangle, |\mathbf{1}_i\rangle\}$ form τ^z eigenbasis of the spin-1/2 particle at the i th site of the 1D lattice of size N . Eigenstates of the 1D model, $|\tilde{\Phi}_l\rangle$, can be written in terms of the $\{|\mathbf{0}_i\rangle, |\mathbf{1}_i\rangle\}$ basis of the spins in the system.

Note 2. A couple of comments about the notations used in the rest of the paper is in order here.

- (a) Any state $|\tilde{\Phi}\rangle$ satisfying $P_g |\tilde{\Phi}\rangle = |\tilde{\Phi}\rangle$ is essentially a state in the 1D XXZ model, which can be written in terms of $|\mathbf{0}\rangle$ and $|\mathbf{1}\rangle$. We will typically put $\tilde{}$ on such states to remind us that it is an XXZ state. Note that the projection of a state $|\Phi\rangle$ onto the low energy sector is $P_g |\Phi\rangle$.
- (b) Similarly, any operator \tilde{A} satisfying $P_g \tilde{A} P_g = \tilde{A}$ is essentially an operator defined on the Hilbert space of the 1D XXZ model, which can be written in terms of $\tau^{x,y,z}$. We will typically put $\tilde{}$ on such operator to remind us that it is an XXZ operator. This also applies to the state ρ , which is a Hermitian operator. Note that the projection of an operator A onto the low energy sector is $P_g A P_g$.

C. Merit of the mapping

We now ask how well the low-energy spectrum of the 2D model is captured by the 1D effective Hamiltonian \tilde{H} . In Sec. II B, we see that for $h = h'$ and $\Delta h = J_{\parallel} = J_d^{1,2} = 0$, the Hilbert space of the system naturally splits into two subspaces - (a) the low-energy subspace \mathcal{S} , spanned by the orthonormal degenerate states $\{|\Psi_l\rangle\}$, where each of the state $|\Psi_l\rangle$ has zero energy w.r.t. H_0 , and (b) the excited subspace \mathcal{S}' , spanned by the excited eigenstates $\{|\Psi'_\alpha\rangle\}$ of H_0 with energy $E'_\alpha \geq \mathcal{O}(J_{\perp})$, where $\langle\Psi'_\alpha|\Psi_l\rangle = 0 \forall l, \alpha$. The total state-space of the system is given by $\mathcal{S} \oplus \mathcal{S}'$. We are now interested in the spectrum of the system slightly away from the point $h = h'$ in the space of coupling constants i.e. $\Delta h, J_{\parallel}, J_d^{1,2} \ll J_{\perp}$. Perturbation theory in the parameter $1/J_{\perp}$ gives the following structure for the energy eigenvalues and eigenvectors of the 2D model:

$$|\Phi_l\rangle = |\Phi_l^0\rangle + J_{\perp}^{-1} |\Phi_l^1\rangle + J_{\perp}^{-2} |\Phi_l^2\rangle + \dots \quad (24)$$

$$E_l = E_l^{(1)} + J_{\perp}^{-1} E_l^{(2)} + \dots \quad (25)$$

where $|\Phi_l^0\rangle$ and $E_l^{(1)}$ are respectively the *non-degenerate*³ eigenvectors and eigenvalues of \tilde{H} . This makes it explicit that the low lying spectrum of the 2D Hamiltonian are very close (upto $1/J_{\perp}$ corrections) to the XXZ spectrum. To see that the eigenstates also match, note that the first order perturbation theory gives the first-order state corrections $|\Phi_l^1\rangle$ to have overlaps with the excited state manifold $\{|\Psi'_\alpha\rangle\}$ having energy of $\mathcal{O}(J_{\perp})$, implying that $|\Phi_l^1\rangle$ is a small correction to $|\Phi_l\rangle$ in Eq. (24) due to the suppression factor J_{\perp}^{-1} . One may quantify the small corrections via the *distance* between $|\Phi_l\rangle$ and $|\Phi_l^0\rangle$, which can be quantified by a distance metric, eg. the *trace-distance* [2] (see Appendix C for definition).

In the following, we describe four instances where the mapping described in Sec. II B is particularly useful.

1. States made of non-degenerate eigenstates

A state in the Hilbert space of the 2D model, which can be written in terms of the non-degenerate eigenstates of H as

$$\rho = \sum_{l,l'} c_{l,l'} |\Phi_l\rangle \langle\Phi_{l'}|, \quad (26)$$

with $\sum_l |c_{l,l}|^2 = 1$, can be approximated as

$$\rho \approx \sum_{l,l'} c_{l,l'} |\Phi_l^0\rangle \langle\Phi_{l'}^0| = \tilde{\rho}, \quad (27)$$

as long as the overall accumulated error due to the first order corrections in $|\Phi_l\rangle \langle\Phi_{l'}|$ is $\leq \mathcal{O}(J_{\perp}^{-1})$ ⁴. We remind ourselves here that $\tilde{\rho}$ is a density matrix entirely in the low energy sector (see **Note 2**, Sec. II B). As an example, consider

the state

$$\rho = \frac{1}{2} \left[|\Phi_0\rangle \langle\Phi_0| + |\Phi_{2^N-1}\rangle \langle\Phi_{2^N-1}| + |\Phi_0\rangle \langle\Phi_{2^N-1}| + |\Phi_{2^N-1}\rangle \langle\Phi_0| \right] \quad (28)$$

of the 2D model, where $|\Phi_0\rangle$ and $|\Phi_{2^N-1}\rangle$ are non-degenerate eigenstates of H ⁵. This state can be approximated as

$$\rho \approx \tilde{\rho} = \frac{1}{2} \left[|\Phi_0^0\rangle \langle\Phi_0^0| + |\Phi_{2^N-1}^0\rangle \langle\Phi_{2^N-1}^0| + |\Phi_0^0\rangle \langle\Phi_{2^N-1}^0| + |\Phi_{2^N-1}^0\rangle \langle\Phi_0^0| \right] \quad (29)$$

up to the correction $\mathcal{O}(J_{\perp}^{-1})$. Since $|\Phi_0^0\rangle = \otimes_i |\psi_0^{(i)}\rangle$, and $|\Phi_{2^N-1}^0\rangle = \otimes_i |\psi_1^{(i)}\rangle$, $\tilde{\rho}$ can be written as $\tilde{\rho} = |\tilde{\Phi}_{\text{GHZ}}\rangle \langle\tilde{\Phi}_{\text{GHZ}}|$ in the space of the 1D effective model, where

$$|\tilde{\Phi}_{\text{GHZ}}\rangle = \frac{1}{\sqrt{2}} \left[|\mathbf{0}^{\otimes N}\rangle + |\mathbf{1}^{\otimes N}\rangle \right] \quad (30)$$

is the N -qubit GHZ state [99, 100]. Note that for ferromagnetic couplings $\tilde{J}_{xy}, \tilde{J}_{zz} < 0$ and for $\tilde{h} > 0$, $|\mathbf{0}\rangle^{\otimes N}$ and $|\mathbf{1}\rangle^{\otimes N}$ represent the ground state and the highest energy eigenstate of \tilde{H} respectively.

2. Equal mixture of degenerate states

Let us now assume that the energy level $E_{l'}^{(1)}$ of \tilde{H} is n -fold degenerate, where the eigenstates of \tilde{H} corresponding to $E_{l'}^{(1)}$ are $|\Phi_{l',m}^0\rangle$, with the index m running from 1 to n . This leads to an n -fold degeneracy of the energy level $E_{l'}$ of H with degenerate eigenstates $|\Phi_{l',m}\rangle$ in first order perturbation theory. Although $|\Phi_{l',m}^0\rangle$ does not approximate the states $|\Phi_{l',m}\rangle$ up to small corrections, the total contribution of the degenerate manifold $\{|\Phi_{l',m}\rangle\}$ in the density matrix at the low-energy sector is approximated by the contribution of the $\{|\Phi_{l',m}^0\rangle\}$. More precisely, the contribution is represented by an equal mixture of the degenerate states $\{|\Phi_{l',m}\rangle\}$ in the Hilbert space of the 2D model, given by

$$\rho = \frac{1}{n} \sum_{m=1}^n |\Phi_{l',m}\rangle \langle\Phi_{l',m}|, \quad (31)$$

which is approximated, up to corrections of $\mathcal{O}(J_{\perp}^{-1})$, by an equal mixture of the corresponding degenerate states $\{|\Phi_{l',m}^0\rangle\}$, i.e.,

$$\rho \approx \tilde{\rho} = \frac{1}{n} \sum_{m=1}^n |\Phi_{l',m}^0\rangle \langle\Phi_{l',m}^0|. \quad (32)$$

³ Degenerate eigenstates of \tilde{H} would result in degeneracy in the energy levels of the 2D model, which can be lifted by second, or higher order perturbation theory.

⁴ This can be ensured by keeping the number of terms in ρ small.

⁵ Here we work in a subspace of the space of coupling constants in H where $|\Phi_0\rangle$ and $|\Phi_{2^N-1}\rangle$ are non-degenerate.

3. Thermal states

Consider the thermal state,

$$\rho_T = \frac{\sum_{\alpha} e^{-\beta E_{\alpha}} |\Phi_{\alpha}\rangle \langle \Phi_{\alpha}|}{\sum_{\alpha} e^{-\beta E_{\alpha}}}, \quad (33)$$

of the 2D system at an absolute temperature $k_B T$, with k_B being the Boltzmann constant, and $\beta = 1/k_B T$, where $\{|\Phi_{\alpha}\rangle\}$ is the full spectrum of H . For low temperatures such that $k_B T \ll \mathcal{O}(J_{\perp})$ (or, $1 \ll \beta J_{\perp}$), the state is well-approximated by the low-energy spectrum as

$$\begin{aligned} \rho_T &\approx \frac{\sum_{l=0}^{2^N-1} e^{-\beta E_l} |\Phi_l\rangle \langle \Phi_l|}{\sum_{l=0}^{2^N-1} e^{-\beta E_l}} \\ &\approx \frac{\sum_{l=0}^{2^N-1} e^{-\beta E_l^{(1)}} |\Phi_l^0\rangle \langle \Phi_l^0|}{\sum_{l=0}^{2^N-1} e^{-\beta E_l^{(1)}}} \\ &= \tilde{\rho}, \end{aligned} \quad (34)$$

up to correction of $\mathcal{O}(1/J_{\perp})$. In the first approximation above, we have truncated the sum to states with $E \ll \mathcal{O}(J_{\perp})$ and in the second, we have approximated both the states and the energies by their XXZ counterparts.

4. Closed system evolution

The mapping of the 2D model to the effective 1D XXZ model also allows one to investigate the time-evolution $\rho(t)$ of the closed system as long as the initial state $\rho(0)$ is of the type described in Eq. (26). Such a state in the Hilbert space of the 2D model evolves as

$$\begin{aligned} \rho(t) &= \sum_{l,l'} c_l c_{l'}^* e^{-i(E_l - E_{l'})t} |\Phi_l\rangle \langle \Phi_{l'}| \\ &\approx \sum_{l,l'} c_l c_{l'}^* e^{-i(E_l^{(1)} - E_{l'}^{(1)})t} |\Phi_l^0\rangle \langle \Phi_{l'}^0| \\ &= \tilde{\rho}, \end{aligned} \quad (35)$$

up to a correction of $\mathcal{O}(1/J_{\perp})$ as long as $t \leq J_{\perp}$.

Note that all the density matrices which we described above, have the property that

$$\rho \approx P_g \rho P_g, \quad (36)$$

implying that these density matrices are approximately the same as their projection onto the low energy sector.

In this paper, we focus on a number of *typical* Hermitian operators and entanglement in the 2D model, and ask to what extent their quantitative as well as qualitative behaviour are approximated by the 1D XXZ model. For this investigation, it is important to work out the effective couplings of \tilde{H} in terms of the original couplings in H , which depends explicitly on the boundary conditions of the 2D lattice. In this respect, one may consider four possible cases – (1) PBC along both rungs and legs, (2) PBC along the rungs and OBC along the legs, (3) OBC along the rungs and PBC along the legs, and (4) OBC along both rungs and legs, all of which we

discuss in detail in Sec. III. Readers interested in the properties of expectation values of relevant operators and entanglement can skip Sec. III, and proceed directly to Secs. IV and V, where these results are discussed.

III. WORKING OUT THE EFFECTIVE HAMILTONIAN

In this section, we explicitly work out the low-energy effective Hamiltonian (21) for different boundary conditions along the legs and rungs. For brevity, we have assumed $J_{\perp} = 1$ only for this section.

A. Periodic boundary condition along the rungs

For the case of PBC along the rungs, given by $\vec{\sigma}_{i,L+1} \equiv \vec{\sigma}_{i,1}$, we present below analytical forms of the ground states $|\psi_k^{(i)}\rangle$, $k = 0, 1$ of the rung Hamiltonian H_{R_i} . This in turn helps us to get analytic expressions for the couplings of effective Hamiltonian.

From the Hamiltonian H_{R_i} given in Eq. (4) (recall that we have set $J_{\perp} = 1$), it is obvious that for large h , the minimum energy state is given by all up spins

$$|\psi_0^{(i)}\rangle = \otimes_{j=1}^L |0_{i,j}\rangle, \quad (37)$$

having energy $L(\frac{1}{4} - \frac{h}{2}) - E_g$. The next higher energy states at large h are given by one spin flip - since this can occur at any of the L rung sites, there are L such states. Since the Hamiltonian H_{R_i} is translationally invariant, we can switch to momentum basis via

$$|q\rangle = \frac{1}{\sqrt{L}} \sum_{j=1}^L e^{2iqj\pi/L} \sigma_{i,j}^x |\psi_0^{(i)}\rangle, \quad (38)$$

where $q = 0, 1, 2, \dots, L-1$. These states are energy eigenstates for all values of h , i.e

$$H_{R_i} |q\rangle = \left[\cos\left(\frac{2\pi q}{L}\right) + L\left(\frac{1}{4} - \frac{h}{2}\right) + h - 1 - E_g \right] |q\rangle. \quad (39)$$

For even L ⁶, the minimum energy eigenstate corresponds to $q = L/2$, with energy eigenvalue $L(\frac{1}{4} - \frac{h}{2}) + h - 2 - E_g$. This state becomes degenerate with the minimum energy state at

$$h' = 2, \quad (40)$$

while the state itself is given by

$$|\psi_1^{(i)}\rangle = |q = L/2\rangle = \frac{1}{\sqrt{L}} \sum_{j=1}^L (-1)^j |j\rangle. \quad (41)$$

⁶ For odd L , the minimum energy states in this sector correspond to $(L \pm 1)/2$. This leads to a three-fold degeneracy of ground states of the rung at $h = h'$, which is beyond the scope of our consideration in this paper.

We must comment here that while it is reasonable to expect that the first excited state at large h becomes degenerate with the minimum energy state as we dial down h , it is not guaranteed to be. However, our numerical investigation verifies this expectation to be correct.

In order to compute parameters of the effective 1d XXZ \tilde{J}_{xy} , \tilde{J}_{zz} , \tilde{h} (see Eq. (21)), we will match the matrix elements of H and \tilde{H} in the following states:

$$\begin{aligned} |\Psi_0\rangle &= \otimes_{i=1}^N |\psi_0^{(i)}\rangle, \\ |\Psi_j\rangle &= |\psi_1^{(j)}\rangle \otimes_{\substack{i=1 \\ i \neq j}}^N |\psi_0^{(i)}\rangle, \\ |\Psi_{j,j+1}\rangle &= |\psi_1^{(j)}\rangle \otimes |\psi_1^{(j+1)}\rangle \otimes_{\substack{i=1 \\ i \neq j, j+1}}^N |\psi_0^{(i)}\rangle. \end{aligned} \quad (42)$$

By matching the matrix elements, the expressions for \tilde{J}_{xy} , \tilde{J}_{zz} , and \tilde{h} can be obtained in terms of the original couplings of the model for PBC along the legs ($\tilde{\sigma}_{N+1,j} \equiv \tilde{\sigma}_{1,j}$) as

$$\begin{aligned} \tilde{J}_{xy} &= (J_{||} - J_d^1 - J_d^2)/4, \\ \tilde{J}_{zz} &= (J_{||} + J_d^1 + J_d^2)/4L, \\ \tilde{h} &= ((L-1)(J_{||} + J_d^1 + J_d^2) - L\Delta h)/2L. \end{aligned} \quad (43)$$

Note that \tilde{J}_{xy} , \tilde{J}_{zz} , and \tilde{h} are dimensionless numbers, since the J_{\perp}^{-1} factor, having value 1, is implicit in all expressions.

Similar mapping and analysis can also be done when the legs obey open boundary condition (OBC). In this case, the effective 1D model is given by

$$\tilde{H}_{\text{OBC}} = \tilde{H} + \tilde{h}'(\tau_1^z + \tau_N^z), \quad (44)$$

with \tilde{H} as in Eq. (21) with its effective couplings given in Eq. (43), the edge-inhomogeneity in the field strength as

$$\tilde{h}' = -(L-1)(J_{||} + J_d^1 + J_d^2)/4L. \quad (45)$$

Note that for both PBC and OBC along the legs, in the limit $L \rightarrow \infty$, $\tilde{J}_{zz} \rightarrow 0$, implying that the 2D model is mapped to an effective 1D XX model in a transverse magnetic field [101–104], which can be exactly solved via fermionization using the Jordan-Wigner transformation, followed by a Fourier transformation.

B. Open boundary condition along the rungs

Open boundary condition (OBC) along the rungs represents a geometry of the lattice that is different from the one discussed in Sec. III A. Exact calculation of the degenerate ground states and the strength of the magnetic field at which the degeneracy occurs is difficult for arbitrary L . However, our numerical analysis suggests that for open (periodic) boundary condition along the rungs (legs), and for arbitrary L , $|\psi_0^{(i)}\rangle$ is still given by Eq. (37), while $|\psi_1^{(i)}\rangle$ is found in the $\langle Z_i \rangle = L-2$ sector, and has the form

$$|\psi_1^{(i)}\rangle = \sum_{j=1}^L a_j |j\rangle, \quad (46)$$

with $a_j \in \mathbb{R}$, and $\sum_{j=1}^L a_j^2 = 1$. Note further that due to Z_2 symmetry, $a_1 = \pm a_L$. Using Eqs. (37) and (46), the effective couplings in Eq. (21) can be determined as

$$\begin{aligned} \tilde{J}_{xy} &= [J_{||} + A_0(J_d^1 + J_d^2)]/4, \\ \tilde{J}_{zz} &= [(4-L+A_1)J_{||} \\ &\quad + (L-1+A_3-2A_2)(J_d^1 + J_d^2)]/16, \\ \tilde{h} &= [(L-A_1)J_{||} + (L-1-A_3)(J_d^1 + J_d^2) - 2\Delta h]/8, \end{aligned} \quad (47)$$

with

$$A_0 = \sum_{j=1}^{L-1} a_j a_{j+1}, \quad (48)$$

$$A_1 = L \sum_{j=1}^L a_j^4 + (2L-8) \sum_{j=1}^L \sum_{k < j} a_j^2 a_k^2, \quad (49)$$

$$A_2 = L-3 + 2a_1^2, \quad (50)$$

$$\begin{aligned} A_3 &= (L-1) \left\{ \sum_{j=1}^{L-1} a_j^2 a_{j+1}^2 + a_L^2 a_1^2 \right\} \\ &\quad + (L-3) \left\{ \sum_{j=1}^{L-1} a_j^2 a_1^2 + \sum_{j=2}^L a_L^2 a_j^2 \right\} \\ &\quad + (L-5) \left\{ \sum_{j=1}^{L-1} \sum_{k=j+2}^L a_j^2 a_k^2 + \sum_{j=2}^L \sum_{k=j}^{L-1} a_k^2 a_j^2 \right\} \end{aligned} \quad (51)$$

The calculation is involving, and we have demonstrated the important steps in Appendix B.

Similar calculation can also be performed for the case of OBC along the legs, where the 1D LEH picks up an inhomogeneity of the effective magnetic field strength \tilde{h} at the edge spins, so that the effective Hamiltonian now reads (44), where the effective couplings are given in Eq. (47), the edge-inhomogeneity in the field is

$$\tilde{h}' = -[(L-1-A_3)(J_d^1 + J_d^2) + (L-A_1)J_{||}]/16 \quad (52)$$

1. Large L limit

At $L \rightarrow \infty$, the field-strength h' leading to doubly degenerate ground states of the rung approach the same in the case of PBC along the rungs. To demonstrate this numerically, we show that h'_{OBC} asymptotically approaches $h'_{\text{PBC}} = 2$ (see Eq. (40)) as

$$h'_{\text{OBC}} = h'_{\text{PBC}} - \left(\frac{a}{L}\right)^2 + \dots, \quad (53)$$

where a is a constant, and we ignore third and higher order terms in $1/L$ (see Fig. 2(a) for a demonstration).

In order to use the ground state $|\psi_1^{(i)}\rangle$ of the i th rung with PBC as an approximation of the same with OBC along the rungs in the $L \rightarrow \infty$ limit, it is important to investigate up to what extent the former mimics the latter. In this paper, we are interested in the *bulk* of the system located at the middle of

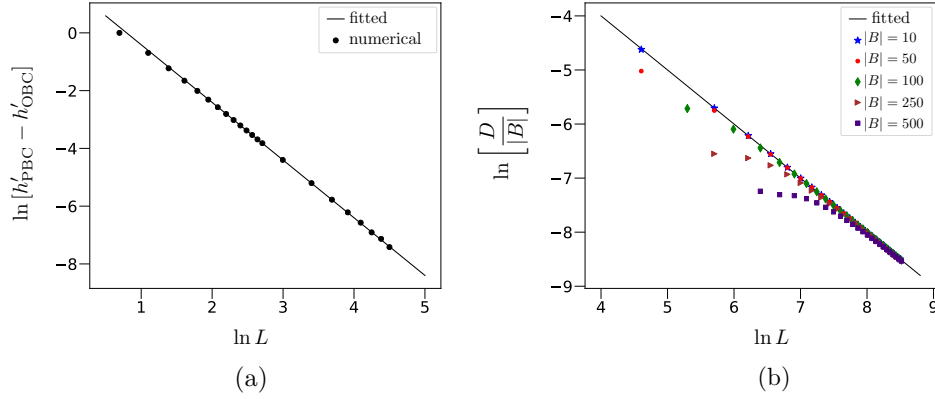


FIG. 2. (a) Variation of $\ln(h'_{\text{PBC}} - h'_{\text{OBC}})$ as a function of $\ln L$. The numerical data is obtained by considering $2 \leq L \leq 10^2$, and is fitted to Eq. (53) with $a = 4.88251$, and the power of L obtained as ~ -1.99684 from the fitted curve. (b) Variation of $\ln[D/|B|]$ as a function of $\ln L$ with different values of $|B|$. The numerical data is obtained by considering $10^2 \leq L \leq 5 \times 10^3$, and is fitted to Eq. (54), where the power of L is obtained as ~ -1.004 from the fitted curve. All quantities plotted in all figures are dimensionless.

the lattice. This naturally includes the bulk B of the rungs at the middle of the lattice, the size $|B|$ of which is determined by the lattice sites included in it. The reduced state ρ_B of the bulk of a rung can be determined by tracing out all spins from $|\psi_1^{(i)}\rangle$ except the ones in the bulk. To quantitatively estimate how ρ_B^{OBC} corresponding to OBC along rungs approaches ρ_B^{PBC} when the rungs form closed chains, we focus on the trace distance [2] (see Appendix C for the definition), D , between ρ_B^{PBC} and ρ_B^{OBC} . Our numerical results indicate that D varies with L as

$$D \sim \frac{|B|}{L}, \quad (54)$$

and tends to 0 for $L \rightarrow \infty$. Here, second and higher powers of $1/L$ are ignored. See Fig. 2(b) for a demonstration. This result indicates that for $L \rightarrow \infty$, a rung with OBC can be reliably mimicked by a rung with PBC as long as the investigation is confined in the bulk of the chain.

2. Mapping for odd L with vanishing magnetic field

We now discuss a special case where L is odd, and no magnetic field is present in the system, i.e., $h = 0$. In this situation, each rung i of the system has a doubly degenerate ground state having the form

$$|\psi_0^{(i)}\rangle = \sum_j a_j \mathcal{P}_j \left(|0\rangle^{\otimes(L+1)/2} |1\rangle^{\otimes(L-1)/2} \right), \quad (55)$$

with $\sum_j a_j^2 = 1$, and

$$|\psi_1^{(i)}\rangle = \otimes_{j=1}^L \sigma_j^x |\psi_0^{(i)}\rangle. \quad (56)$$

Here, $\{\mathcal{P}_j\}$ is the set of all possible permutations of L' ($L - L'$) spins at ground (excited) state, with $L' = (L - 1)/2$ ($L' = (L + 1)/2$) for $|\psi_0^{(i)}\rangle$ ($|\psi_1^{(i)}\rangle$). **Proposition 1** (see Sec. II B) is valid in this case also, and calculation (see Ap-

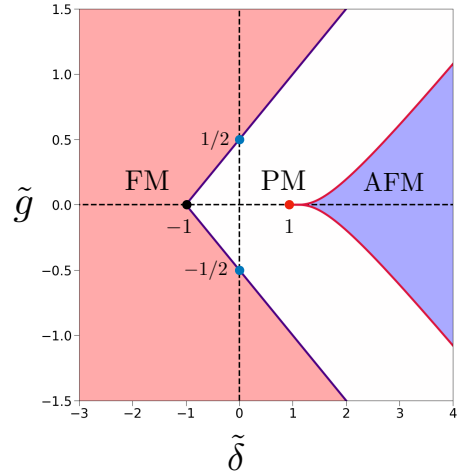


FIG. 3. Phase diagram of the 1D XXZ model in a magnetic field on the plane of $(\tilde{\delta}, \tilde{g})$ [95, 105], marking the antiferromagnetic (AFM), ferromagnetic (FM), and paramagnetic (PM) phases and the corresponding phase boundaries, where $\tilde{\delta} = \tilde{J}_{zz}/\tilde{J}_{xy}$ quantifies the z -anisotropy, and $\tilde{g} = h/\tilde{J}_{xy}$.

pendix D) leads to an effective 1D model given by the Hamiltonian

$$\tilde{H} = \sum_{i=1}^N \left[\tilde{J}_{xy} (\tau_i^x \tau_{i+1}^x + \tau_i^y \tau_{i+1}^y) + \tilde{J}_{zz} \tau_i^z \tau_{i+1}^z \right]. \quad (57)$$

We demonstrate the important steps of the calculation in Appendix D, where we set $J_d^1 = J_d^2 = 0$ to keep the calculation uncluttered. However, similar results can be obtained also for non-zero perturbations J_d^1, J_d^2 , where the overall form of Eq. (57) remains unchanged.

A	\tilde{A}
$\sigma_{i,j}^\alpha$	$\frac{(-1)^j}{\sqrt{L}}\tau_i^\alpha$, for $\alpha = x, y$
$\sigma_{i,j}^z$	$\frac{L-1}{L}I_i + \frac{1}{L}\tau_i^z$
$\sum_{j=1}^L \sigma_{i,j}^z$	$(L-1)I_i + \tau_i^z$
$\sum_{j=1}^L \sigma_{i,j}^x$	0
$\sum_{j=1}^L \sigma_{i,j}^y$	0
$\otimes_{j=1}^L \sigma_{i,j}^z$	τ_i^z
$\otimes_{j=1}^L \sigma_{i,j}^x$	$\frac{1}{2}(\tau_i^z - I_i)$ for $L = 2$ 0 for $L > 2$
$\otimes_{j=1}^L \sigma_{i,j}^y$	$\frac{1}{2}(\tau_i^z - I_i)$ for $L = 2$ 0 for $L > 2$
$\sigma_{i,1}^x \otimes \sigma_{i,2}^z$	$-\frac{1}{\sqrt{2}}\tau_i^x$
$\sigma_{i,1}^z \otimes \sigma_{i,2}^x$	$\frac{1}{\sqrt{2}}\tau_i^x$
$\sigma_{i,1}^y \otimes \sigma_{i,2}^z$	$-\frac{1}{\sqrt{2}}\tau_i^y$
$\sigma_{i,1}^z \otimes \sigma_{i,2}^y$	$\frac{1}{\sqrt{2}}\tau_i^y$
$\sigma_{i,1}^x \otimes \sigma_{i,2}^y$	0
$\sigma_{i,1}^y \otimes \sigma_{i,2}^x$	0
$\sigma_{i,j}^\alpha \otimes \sigma_{i+r,j'}^\alpha$	$\frac{(-1)^{j+j'}}{L}\tau_i^\alpha \otimes \tau_{i+r}^\alpha$ for $\alpha = x, y$
$\sigma_{i,j}^z \otimes \sigma_{i+r,j'}^z$	$\frac{(L-1)^2}{L^2}I + \frac{1}{L^2}\tau_i^z \tau_{i+r}^z + \frac{L-1}{L^2}(\tau_i^z + \tau_{i+r}^z)$
$\sigma_{i,j}^x \otimes \sigma_{i+r,j'}^z$	$\frac{(-1)^j}{\sqrt{L}} \left[\frac{L-1}{L}\tau_i^x + \frac{1}{L}\tau_i^x \tau_{i+r}^z \right]$
$\sigma_{i,j}^z \otimes \sigma_{i+r,j'}^x$	$\frac{(-1)^{j'}}{\sqrt{L}} \left[\frac{L-1}{L}\tau_{i+r}^x + \frac{1}{L}\tau_i^z \tau_{i+r}^x \right]$
$\sigma_{i,j}^y \otimes \sigma_{i+r,j'}^z$	$\frac{(-1)^j}{\sqrt{L}} \left[\frac{L-1}{L}\tau_i^y + \frac{1}{L}\tau_i^y \tau_{i+r}^z \right]$
$\sigma_{i,j}^z \otimes \sigma_{i+r,j'}^y$	$\frac{(-1)^{j'}}{\sqrt{L}} \left[\frac{L-1}{L}\tau_{i+r}^y + \frac{1}{L}\tau_i^z \tau_{i+r}^y \right]$
$\sigma_{i,j}^x \otimes \sigma_{i+r,j'}^y$	0
$\sigma_{i,j}^y \otimes \sigma_{i+r,j'}^x$	0

TABLE I. A list of typical observables on the ladder and the corresponding low-energy operators on the 1D effective XXZ model, where PBC along both rungs and legs have been used for calculation. A subset of these operators for $L = 2$ can be found in [89].

IV. MAPPING OBSERVABLES

It has been seen in Sec. II that specific states in the low-energy sector of the 2D model (1) is approximated, up to corrections of $\mathcal{O}(1/J_\perp)$, by the spectrum of the 1D effective XXZ model. A natural question that arises at this point is *whether the low energy content of an observable (i.e., matrix elements of Hermitian operators in the low energy subspace) are captured by an observable defined entirely on the Hilbert space of the 1D effective XXZ model?* We answer this question affirmatively below.

To put the question in a more concrete mathematical footing, we focus on the matrix element $\langle \Phi_l | A | \Phi_{l'} \rangle$ of a Hermitian operator A on the space of the non-degenerate low energy states of the 2D model, and ask whether there exists a Hermitian operator \tilde{A} on the space of the 1D XXZ model

such that

$$\langle \Phi_l | A | \Phi_{l'} \rangle \approx \langle \Phi_l^0 | \tilde{A} | \Phi_{l'}^0 \rangle, \quad (58)$$

Towards answering this question, we note that an alternative definition for P_g would be $P_g = \sum_l |\Phi_l^0\rangle \langle \Phi_l^0|$, which is better suited for subsequent discussion. Equipped with this, we propose the following.

Proposition 2. *Eq. (58) holds if $\tilde{A} = P_g A P_g$.*

Proof. To prove this, let us write

$$\begin{aligned} \langle \Phi_l | A | \Phi_{l'} \rangle &= \langle \Phi_l | P_g A P_g | \Phi_{l'} \rangle + \langle \Phi_l | P_e A P_g | \Phi_{l'} \rangle \\ &\quad + \langle \Phi_l | P_g A P_e | \Phi_{l'} \rangle + \langle \Phi_l | P_e A P_e | \Phi_{l'} \rangle, \end{aligned} \quad (59)$$

and note that for the low-energy manifold of H ,

$$P_g | \Phi_{l'} \rangle = \sum_l |\Phi_l^0\rangle \langle \Phi_l^0 | \Phi_{l'} \rangle \approx |\Phi_{l'}^0\rangle, \quad (60)$$

since for $l \neq l'$, $\langle \Phi_l^0 | \Phi_{l'} \rangle \rightarrow 0$ due to Eq. (24) and orthonormality of $|\Phi_l^0\rangle$. Also note that $P_e | \Phi_{l'} \rangle \approx P_e | \Phi_{l'}^0 \rangle = 0$. Therefore,

$$\langle \Phi_l | A | \Phi_{l'} \rangle \approx \langle \Phi_l | P_g A P_g | \Phi_{l'} \rangle = \langle \Phi_l^0 | \tilde{A} | \Phi_{l'}^0 \rangle, \quad (61)$$

where $\tilde{A} = P_g A P_g$. Hence proved. \square

We point out here that although the proof is presented for non-degenerate eigenstates, it can be straightforwardly extended to the states constructed out of the non-degenerate eigenstates discussed in Sec. II C.

We now focus on a number of relevant operators A on the space of the 2D model, and determine the corresponding operators \tilde{A} for the 1D effective model. We assume PBC along both rungs and legs for demonstration. However, the prescription can also be applied to other boundary conditions along legs and rungs. We consider mainly two types of operators – (a) operators A having support only on one rung, say, i , where the corresponding operator $\tilde{A}_i^\alpha = P_g A_i P_g$ is a 2×2 matrix in the $\{|0\rangle, |1\rangle\}$ basis, and has support on only the i th lattice site of the 1D XXZ model, and (2) operators of the form $A_{i,i'} = A_i \otimes A_{i'}$ having support on two different rungs, i , and i' , where the mapped operator $\tilde{A}_{i,i'}$ is a 4×4 Hermitian matrix in the basis $\{|00\rangle, |01\rangle, |10\rangle, |11\rangle\}$ on the spins (i, i') in the 1D XXZ spin-chain. To determine the low-energy component of operators of the latter type, we note the following.

Proposition 3. *For an operator on the space of the 2D model having the form $A_{i,i'} = A_i \otimes A_{i'}$ with A_i and $A_{i'}$ having support only on rungs i and i' respectively, $\tilde{A}_{i,i'} = P_g A_{i,i'} P_g = \tilde{A}_i \otimes \tilde{A}_{i'}$, where $\tilde{A}_i = P_g A_i P_g$, and $\tilde{A}_{i'} = P_g A_{i'} P_g$.*

Proof. To prove this, we write $P_g = \otimes_{i=1}^N P_g^{(i)}$, with $P_g^{(i)} = \sum_{k_i=0}^1 |\psi_{k_i}^{(i)}\rangle \langle \psi_{k_i}^{(i)}|$, where we use notations introduced in Eq. (7). This leads to

$$\begin{aligned} \tilde{A}_{i,i'} &= P_g A_{i,i'} P_g \\ &= [P_g^{(i)} \otimes P_g^{(i')}] (A_i \otimes A_{i'}) [P_g^{(i)} \otimes P_g^{(i')}] \\ &= [P_g^{(i)} A_i P_g^{(i)}] \otimes [P_g^{(i')} A_{i'} P_g^{(i')}] \\ &= \tilde{A}_i \otimes \tilde{A}_{i'}. \end{aligned} \quad (62)$$

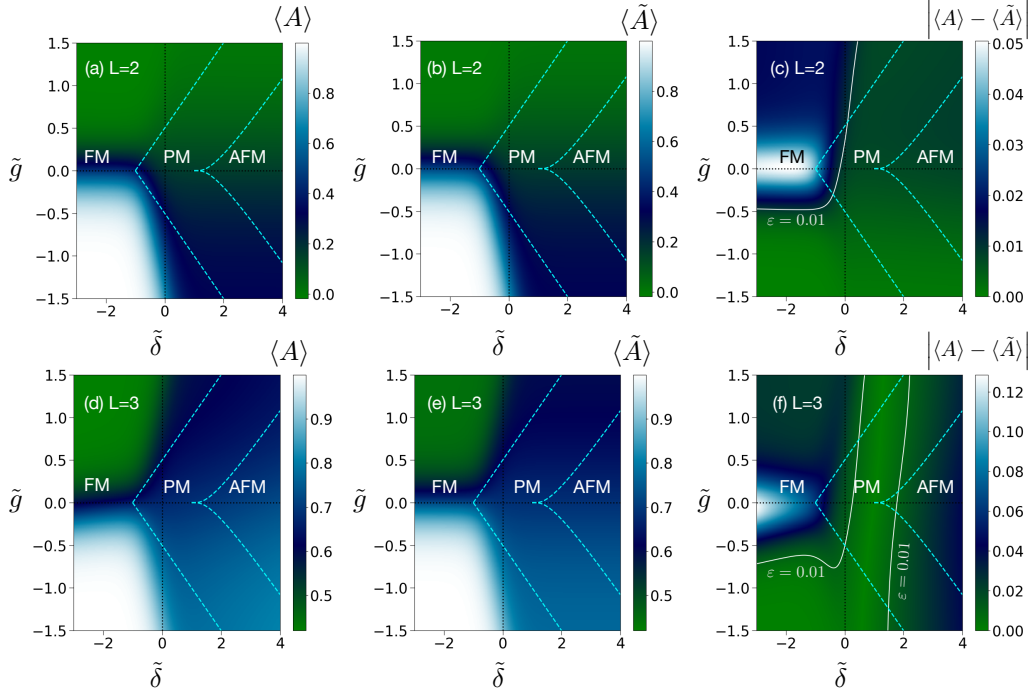


FIG. 4. Variations of $\langle A \rangle$, $\langle \tilde{A} \rangle$, and $\varepsilon = |\langle A \rangle - \langle \tilde{A} \rangle|$ as functions of $\tilde{\delta}$ and \tilde{g} , where $A = \sigma_{i,1}^z \otimes \sigma_{i+1,1}^z$, $\tilde{A} = (I + \tau_i^z + \tau_{i+1}^z + \tau_i^z \otimes \tau_{i+1}^z)/4$ for $L = 2$, and $\tilde{A} = [25I + 5(\tau_i^z + \tau_{i+1}^z) + \tau_i^z \otimes \tau_{i+1}^z]/36$ for $L = 3$. All quantities plotted are dimensionless.

Here we have been explicit only about projectors in the rungs i and i' . Hence the proof. \square

Note that this proposition can be extended to any operator on the space of the 2D model, since it can always be written as a linear combination of tensor products of operators localized on rungs.

We now specifically consider four constructions of A , namely, $\sigma_{i,j}^\alpha$, $\sum_{j=1}^L \sigma_{i,j}^\alpha$, $\otimes_{j=1}^L \sigma_{i,j}^{\alpha_j}$ ⁷, and $\sigma_{i,j}^\alpha \otimes \sigma_{i+r,j'}^{\alpha+r}$, where $\alpha, \alpha_i \in \{x, y, z\}$. The expressions for the corresponding low-energy components \tilde{A} on the 1D XXZ model are given in Table I. For ease of reference, we call the operators A having vanishing low-energy component (i.e., $\tilde{A} = 0$) as *high-energy operators*. Note here that the low-energy component of $\sigma_{i,j}^\alpha$, $\alpha = x, y, z$, is consistent with the operator identification of J_i^z in terms of τ_i^z , as given in Eq. (17) and Eq. (18).

To systematically test the performance of the first-order approximation for the operators listed in Table I, we consider the situation of PBC along the legs⁸. Note that the 1D effective model can be described by two independent dimensionless parameters, $\tilde{g} = \tilde{h}/\tilde{J}_{xy}$, and $\tilde{\delta} = \tilde{J}_{zz}/\tilde{J}_{xy}$, where the dimensionless parameter $\tilde{J}_{xy} \neq 0$, and the physics of the model is expected to be invariant with a change in the value of \tilde{J}_{xy} . Using \tilde{g} and $\tilde{\delta}$, the phase diagram of the 1D XXZ model is given by Fig. 3, where the ferromagnetic

(FM), antiferromagnetic (AFM), and the paramagnetic (PM) phases and the corresponding phase boundaries are marked. We use this phase diagram for reference during discussion of results in subsequent sections. The effective coupling constants are functions of $J_{||}/J_{\perp}$, $J_d^{1,2}/J_{\perp}$, and $\Delta h/J_{\perp}$ (see Eqs. (43) and (47)). Let us define $J_d^{\text{sum}} = |(J_d^1 + J_d^2)/J_{\perp}|$, $J_d^{\text{diff}} = |(J_d^1 - J_d^2)/J_{\perp}|$, and observe that \tilde{J}_{xy} , \tilde{J}_{zz} , and \tilde{h} depend only on J_d^{sum} , and are independent of J_d^{diff} . Solving for $J_{||}/J_{\perp}$, $J_d^{\text{sum}}/J_{\perp}$, and $\Delta h/J_{\perp}$ from Eq. (43), one can write

$$\begin{aligned} \frac{J_{||}}{J_{\perp}} &= 2\tilde{J}_{xy}(L\tilde{\delta} + 1), \quad \frac{J_d^{\text{sum}}}{J_{\perp}} = 2\tilde{J}_{xy}(L\tilde{\delta} - 1), \\ \frac{\Delta h}{J_{\perp}} &= 2\tilde{J}_{xy}[2(L-1)\tilde{\delta} - \tilde{g}], \end{aligned} \quad (63)$$

for PBC along the rungs. In the case of OBC along the rungs, from Eq. (47), one obtains

$$\begin{aligned} \frac{J_{||}}{J_{\perp}} &= \frac{4\tilde{J}_{xy}(4A_0\tilde{\delta} + C_1)}{C_1 + A_0C_2}, \quad \frac{J_d^{\text{sum}}}{J_{\perp}} = \frac{4\tilde{J}_{xy}(C_2 - 4\tilde{\delta})}{C_1 + A_0C_2}, \\ \frac{\Delta h}{J_{\perp}} &= 2\tilde{J}_{xy} \left[\frac{(4 - C_2)(4A_0\tilde{\delta} + C_1)}{C_1 + A_0C_2} \right. \\ &\quad \left. + \frac{2(A_2 - A_3)(C_2 - 4\tilde{\delta})}{C_1 + A_0C_2} - 4\tilde{g} \right], \end{aligned} \quad (64)$$

where $C_1 = 2A_2 - A_3 - L + 1$, $C_2 = 4 - L + A_1$, and A_0, A_1, A_2 , and A_3 are given in Eqs. (48)-(51). In the following, we consider expectation values of specific Hermitian operators, both in the 2D model as well as in the effective 1D model, as functions of \tilde{g} and $\tilde{\delta}$, under the constraints that the corresponding $(J_{||}/J_{\perp}, J_d^{\text{sum}}/J_{\perp}, J_d^{\text{diff}}/J_{\perp}, \Delta h/J_{\perp})$ are small.

⁷ One might naively guess that if A_i, B_i maps to \tilde{A}_i, \tilde{B}_i in XXZ model, then for $C_i = A_i B_i$ the corresponding XXZ operator is $\tilde{C}_i = \tilde{A}_i \tilde{B}_i$.

However this is not true - see Eq. (62) for the caveat.

⁸ OBC along the legs can also be considered in similar fashion.

Note that irrespective of the value of $\tilde{\delta}$ and \tilde{g} , this can be ensured by fixing \tilde{J}_{xy} to a small value⁹. We fix $\tilde{J}_{xy} = 10^{-2}$ and $J_d^{\text{diff}} = 0$ for the range $-3 \leq \tilde{\delta} \leq 4$ and $-1.5 \leq \tilde{g} \leq 1.5$ considered in this work.

For demonstration, we choose $A = \sigma_{i,1}^z \otimes \sigma_{i+1,1}^z$ on a 3×2 and 3×3 lattice, for which the low-energy component \tilde{A} is given in Table I. We compute $\langle A \rangle = \text{Tr}(\rho A)$ and $\langle \tilde{A} \rangle = \text{Tr}(\tilde{\rho} \tilde{A})$, where ρ and $\tilde{\rho}$ are considered to be a thermal state (see Eq. (34)). To ensure that the state lies in the low-energy sector of the 2D model, we consider $\beta J_{\perp} = 10^2$, where the strength of the rung-coupling is taken to be $J_{\perp} = 10^2$. Fig. 4 depicts the variation of $\langle A \rangle$, $\langle \tilde{A} \rangle$, and $\varepsilon = |\langle A \rangle - \langle \tilde{A} \rangle|$ as functions of $\tilde{\delta}$ and \tilde{g} , where OBC is assumed along the rungs of the lattices. In order to quantitatively estimate the performance of the 1D effective XXZ model to substitute the values of $\langle A \rangle$, on the terrain of ε , we mark the regions in which $\varepsilon \leq J_{\perp}^{-1} = 10^{-2}$. Note that in the case of $L = 2$, major portions of the considered $(\tilde{\delta}, \tilde{g})$ plane is included in this region, with relatively higher values of ε occurring mostly in the FM phase with $\tilde{g} \geq 0$. In contrast, for $L = 3$, higher values of ε appear in the PM and the AFM phases also. These observations remain qualitatively unchanged for observables defined on a single rung instead of two different rungs. For a discussion and demonstration with $A = \sigma_{1,1}^z \otimes \sigma_{2,2}^z$ and $A = \sigma_{i,1}^z$, see Appendix F. We want to emphasise here that that qualitative variations of $\langle A \rangle$ in the 2D model is mimicked satisfactorily by the same for $\langle \tilde{A} \rangle$ in the effective 1D model, in the entire range of $(\tilde{\delta}, \tilde{g})$ considered in this paper, even beyond the realm of perturbation theory.

V. ESTIMATING ENTANGLEMENT

Now that we have matched the spectrum and observables from the 2D model to the 1D XXZ model, in this Section, we focus on quantum correlation measures belonging to the entanglement-separability paradigm [25, 26] that can be computed in the system under consideration.

A. Entanglement from reduced density matrices

While the distribution of entanglement in a quantum spin model can be varied, such as bipartite and multipartite entanglement over different subsystems, it often adapts a partial trace-based methodology for computation [25]. For example, the bipartite entanglement between two subsystems of the spin model in a pure state, is inferred from the reduced density matrix of one of the subsystems. Therefore, the first natural question to address here is if there exists a relation between the reduced density matrices of subsystems of the 2D model, and the reduced density matrices of the corresponding subsystems in the effective 1D XXZ model. In fact, it

is natural to expect that a single-rung reduced density matrix in the 2D model will match to a single spin reduced density matrix in the 1D XXZ model. We will now show that this is indeed true.

Let us begin with a density matrix of the 2D system, which has a description in the 1D effective XXZ model, i.e $\rho \approx P_g \rho P_g = \tilde{\rho}$. For this, we propose the following.

■ **Proposition 4.** *The reduced density matrix $\rho^{(i)}$ obtained via tracing out the rung i from ρ and the reduced density matrix $\tilde{\rho}^{(i)}$ obtained from $\tilde{\rho}$ by tracing out the spin i obeys $\rho^{(i)} \approx \tilde{\rho}^{(i)}$.*

Proof. Note that exploiting the basis-independence of partial trace, and using notations introduced in Eq. (7) in Sec. II B,

$$\rho^{(i)} = \text{Tr}_i \rho = \sum_{k=0}^{2^L-1} \langle \psi_k^{(i)} | \rho | \psi_k^{(i)} \rangle \quad (65)$$

whereas

$$\tilde{\rho}^{(i)} = \text{Tr}_i \tilde{\rho} = \sum_{k=0}^1 \langle \psi_k^{(i)} | \tilde{\rho} | \psi_k^{(i)} \rangle \quad (66)$$

To prove that $\rho^{(i)} \approx \tilde{\rho}^{(i)}$, we consider

$$\langle \psi_k^{(i)} | \rho | \psi_k^{(i)} \rangle \approx \langle \psi_k^{(i)} | \tilde{\rho} | \psi_k^{(i)} \rangle = \langle \psi_k^{(i)} | P_g \rho P_g | \psi_k^{(i)} \rangle \quad (67)$$

Since $P_g = \otimes_i P_g^i$ and $P_g^i | \psi_k^{(i)} \rangle = 0$ unless $k = 0, 1$, it follows that the RHS of (67) is vanishing for $k > 1$. Thus we have that the reduced density matrix on the space of the 2D model (Eq. (65)) becomes

$$\rho^{(i)} \approx \sum_{k=0}^1 \langle \psi_k^{(i)} | \rho | \psi_k^{(i)} \rangle = \tilde{\rho}^{(i)}. \quad (68)$$

Hence proved. \square

The next corollary follows straightforwardly from **Proposition 4**.

◇ **Corollary 4.1.** *The reduced density matrix ρ_S for a subsystem composed of a set S of arbitrary number of rungs obtained from the state ρ of the 2D model and the reduced density matrix $\tilde{\rho}_S$ of the corresponding set S of spins obtained from the state $\tilde{\rho}$ of the 1D XXZ model obeys $\rho_S \approx \tilde{\rho}_S$.*

Proposition 4 and **Corollary 4.1** can be verified by computing the trace distance between ρ_S and $\tilde{\rho}_S$. This implies that any function of the density matrices, for example, entanglement quantified over subsystems using their reduced density matrices, such as the bipartite entanglement between two chosen parties [25, 26], entanglement spectrum [106], distance-based multipartite entanglement [107–109], or multipartite quantum correlation quantified by monogamy-bases approaches [110–117] should also match for ρ_S and $\tilde{\rho}_S$. To demonstrate this, we choose bipartite entanglement over a subsystem S constituted of two nearest-neighbor rungs in the 2D lattice, which corresponds to two nearest-neighbor spins in the 1D effective model. We numerically compute the bipartite entanglement $E_{i,i+1}$, between the two rungs i

⁹ This is the only constraint on \tilde{J}_{xy} , which, in turn, implies that $J_{||}/J_{\perp}$ and $J_d^{\text{sum}}/J_{\perp}$ have to be comparable.

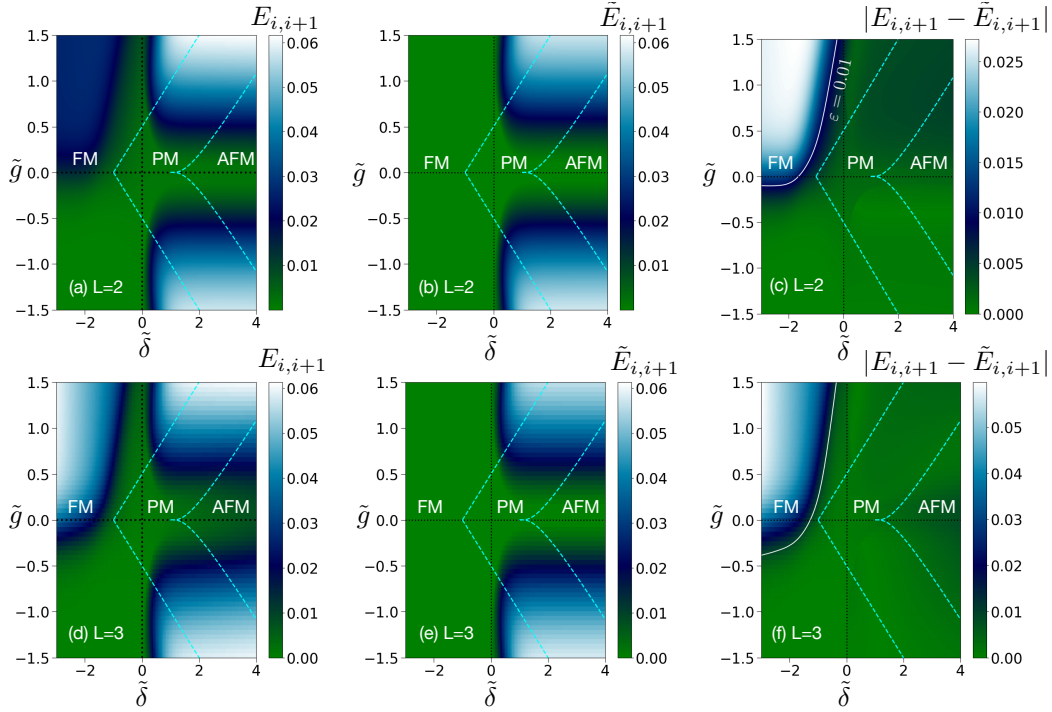


FIG. 5. Variations of $E_{i,i+1}$, $\tilde{E}_{i,i+1}$, and $\varepsilon = |E_{i,i+1} - \tilde{E}_{i,i+1}|$ as functions of $\tilde{\delta}$ and \tilde{g} . The top horizontal panel is for a 3×2 lattice, while figures in the bottom horizontal panel are for a 3×3 lattice. All quantities plotted are dimensionless.

and $i + 1$ in the 2D model from their reduced density matrix $\rho_{i,i+1}$, and the bipartite entanglement $\tilde{E}_{i,i+1}$ between the spins $(i, i + 1)$ in the 1D effective XXZ model from their reduced density matrix $\tilde{\rho}_{i,i+1}$, where negativity [118–124] (see Appendix E for a definition) is used for entanglement quantification. These reduced density matrices $\rho_{i,i+1}$ and $\tilde{\rho}_{i,i+1}$ are obtained respectively by tracing out all other rungs other than the rungs $(i, i + 1)$ from the thermal state ρ of the 2D model, and by tracing out all other spins except the spins i and $i + 1$ from the thermal state $\tilde{\rho}$ of the 1D model (see Sec. II C 3). To ensure low-energy of the states, we fix $\beta J_{\perp} = 10^2$, while $J_{\perp} = 10^2$.

The variations for $E_{i,i+1}$ and $\tilde{E}_{i,i+1}$ as functions of $(\tilde{\delta}, \tilde{g})$ are included in Fig. 5 in the case of a two-leg and a three-leg system. Similar to the expectation values of observables discussed in Sec. IV, to quantitatively test the performance of the 1D effective theory in estimating $E_{i,i+1}$, we look at the variation of $\varepsilon = |E_{i,i+1} - \tilde{E}_{i,i+1}|$ as functions of $\tilde{\delta}$ and \tilde{g} , and find that $\varepsilon \leq J_{\perp}^{-1} = 10^{-2}$ for the whole of the AFM and the PM phases, while relatively high values of ε occurs in the FM phases for $\tilde{g} \geq 0$. These observations remain qualitatively unchanged with a change in the value of L from 2 to 3. To check whether these observations change with a change of the subsystem over which entanglement is computed, or with a change from the bipartite entanglement to a multipartite quantum correlation, we further consider (a) bipartite entanglement, as quantified by negativity, over a bipartition of the entire system, and (b) a monogamy-based [110–114, 117] multipartite quantum correlation, referred to as the monogamy score [115–117], over the entire system, and find the observations reported so far to be valid. See Appendix G

for details. Also, note that for the entirety of the $(\tilde{\delta}, \tilde{g})$ plane considered in this paper, the behaviour of different quantum correlations is qualitatively mimicked by the same for their corresponding XXZ counterparts, although the perturbation theory may not be valid everywhere on the plane.

B. Measurement-based quantification of entanglement

Given a quantum state ρ of a composite quantum system, one may also quantify entanglement over a subsystem using a measurement-based protocol [125–129]. For a bipartition $S : \bar{S}$ of the system, a local projection measurement on one of the subsystems, say, S , leads to an ensemble of post-measured states $\varrho_{S\bar{S}}^{(i)} = P_S^{(i)} \rho_{S\bar{S}} P_S^{(i)\dagger} / \text{Tr} [P_S^{(i)} \rho_{S\bar{S}} P_S^{(i)\dagger}]$ with probabilities $p_i = \text{Tr} [P_S^{(i)} \rho_{S\bar{S}} P_S^{(i)\dagger}]$. Here, $P_S^{(i)} = |\psi_S^{(i)}\rangle \langle \psi_S^{(i)}|$, $i = 0, 2, \dots, d_S - 1$ are projection operators corresponding to the eigenkets $|\psi_S^{(i)}\rangle$ of a chosen Hermitian operator M_S on the Hilbert space of S with dimension d_S . For each choice of M_S , one can define average entanglement in the post-measured states of \bar{S} , given by

$$\langle E \rangle_{\bar{S}} = \sum_{i=0}^{d_S-1} p_i E(\varrho_{\bar{S}}^{(i)}), \quad (69)$$

where $\varrho_{\bar{S}}^{(i)} = \text{Tr}_S \varrho_{S\bar{S}}^{(i)}$. Note that the subsystem \bar{S} can be a collection of smaller subsystems, and the entanglement measure E can be either a bipartite, or a multipartite measure. In this work, we choose bipartite entanglement quantified

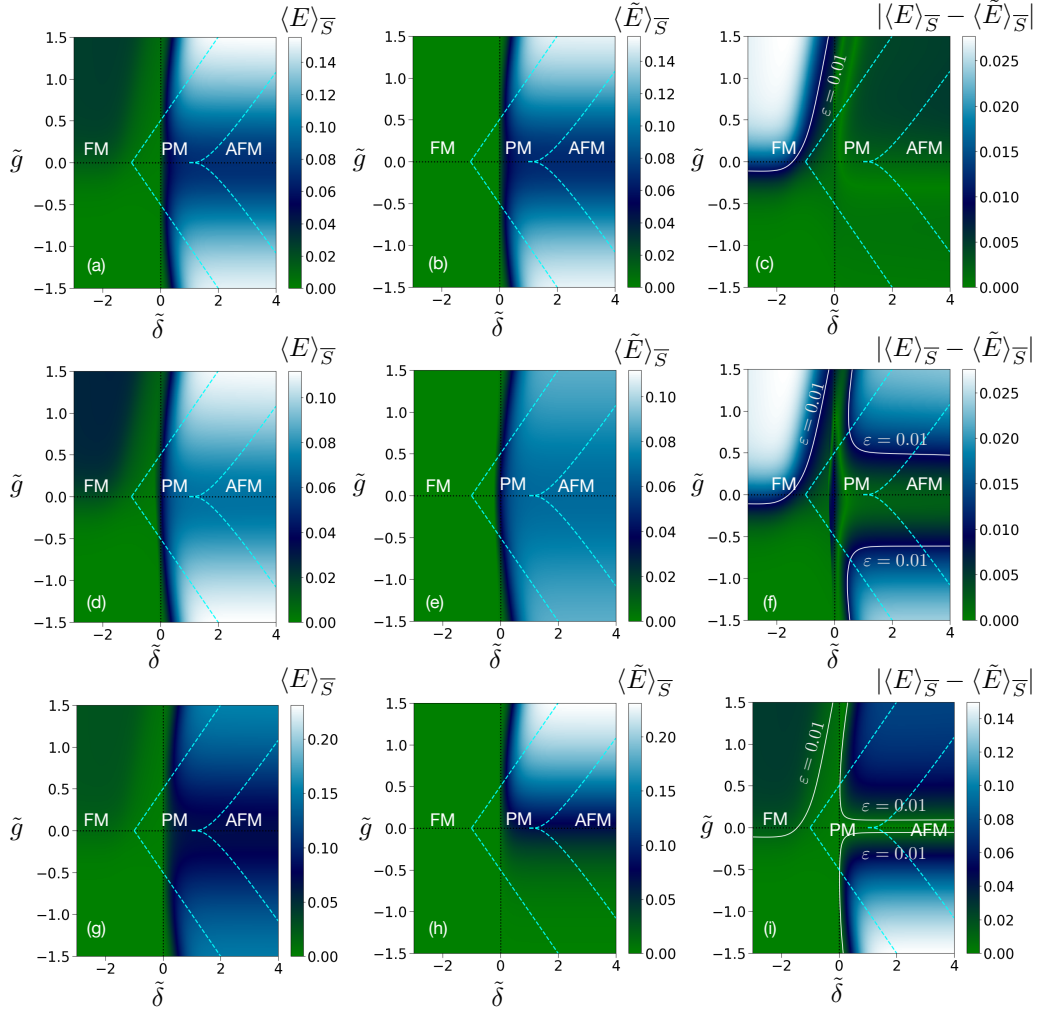


FIG. 6. Variations of $\langle E \rangle_{\bar{S}}$, $\langle \tilde{E} \rangle_{\bar{S}}$, and $\varepsilon = |\langle E \rangle_{\bar{S}} - \langle \tilde{E} \rangle_{\bar{S}}|$ as functions of $\tilde{\delta}$ and \tilde{g} for a 3×2 lattice. The top, middle, and bottom horizontal panels are respectively for the measurement of M_i^{zz} , M_i^{zx} , and M_i^{xx} . All quantities plotted are dimensionless.

by negativity. For a given operator M_S with a low-energy description (i.e., if $P_g M_S P_g \neq 0$), we ask the question as to whether the value $\langle E \rangle_{\bar{S}}$ obtained from a low-energy state $\rho_{\bar{S}}$ of the 2D lattice is approximated by $\langle \tilde{E} \rangle_{\bar{S}}$ via a measurement of \tilde{M}_S in the corresponding state $\tilde{\rho}_{\bar{S}}$ of the 1D XXZ model? We ask this question for two classes of operators - one keeps the low-energy sector invariant, i.e., $P_g M_S P_g = M_S$, and the other which takes a low-energy state out of the low-energy manifold, i.e., $P_g M_S P_g \neq M_S$.

We now identify each S as the rung i , and for demonstration, we choose three examples of single-rung operators, given by $M_i^{zz} = \sigma_{i,1}^z \otimes \sigma_{i,2}^z$ belonging to the first category, and $M_i^{xx} = \sigma_{i,1}^x \otimes \sigma_{i,2}^x$, and $M_i^{zx} = \sigma_{i,1}^z \otimes \sigma_{i,2}^x$ belonging to the second category, with their respective low-energy components given in Table I. For these operators, we compute $\langle E \rangle_{\bar{S}}$ in a $N \times 2$ ladder, $\langle \tilde{E} \rangle_{\bar{S}}$ in the N -spin 1D effective model, and $\varepsilon = |\langle E \rangle_{\bar{S}} - \langle \tilde{E} \rangle_{\bar{S}}|$ for the thermal state (see Sec. II C 3), with $\beta J_{\perp} = 10^2$, where $J_{\perp} = 10^2$. In all our calculations, entanglement in the subsystem \bar{S} is computed over the bipartition 1 rung : rest of the subsystem (1 spin :

rest of the subsystem) in the case of the 2D model (effective 1D model). The behaviours of $\langle E \rangle_{\bar{S}}$, $\langle \tilde{E} \rangle_{\bar{S}}$, and ε , in the case of a 3×2 lattice, as functions of $\tilde{\delta}$ and \tilde{g} , in the case of these single-rung operators are depicted in Fig. 6. It is clear from the figure that the performance of the 1D XXZ model as a proxy for the 2D model worsens as one shifts from the first category of operators to the second. We also point out that in the case of M_i^{zz} , the 1D XXZ model is a good substitute for the 2D model in the entire PM and AFM phases as well as in the FM phase where $\tilde{g} < 0$.

VI. CONCLUSION AND OUTLOOK

In this paper, we consider a spin-1/2 isotropic Heisenberg model in a magnetic field on a rectangular zig-zag lattice of size $N \times L$. We show that in some regimes of system parameters, irrespective of the values of N and L , the 2D model can be well-approximated by an 1D spin-1/2 XXZ model. In particular, we show that for specific states in the low-energy manifold of the 2D model, matrix elements of typical Hermi-

tian operators, and non-local quantum correlations such as entanglement, the 1D XXZ model provides a satisfactory proxy even when the perturbation parameters are not small. We further consider the quantification of measurement-based entanglement, where a measurement over a Hermitian operator is required, and find that the 1D model can mimic the 2D model for certain choices of the Hermitian operators. While we demonstrate these results for low values of N and L , these positive findings open up an opportunity for investigating observables as well as entanglement in the case of 2D models with higher N and L using the 1D XXZ model as a proxy.

We conclude with a discussion on possible future works. An interesting direction would be to generalize the calculation where ground-states of individual rungs have higher degeneracies ($d > 2$), so that 2D models with d degrees of freedom per cite can be addressed. It is also important to ask whether expectation values of Hermitian operators defined on the 2D model for specific purposes, such as order parameters [130, 131], or entanglement witness operators [132, 133], can be estimated using the effective 1D model. Moreover, motivated from the results on measurement-based quantification of entanglement, other quantum correlations belonging to the quantum information-theoretic paradigms [7, 10], such as quantum discord [134, 135] and quantum work deficit [136, 137], requiring measurements on subsystems can be investigated. While our mapping to 1D XXZ model works for specific sites (see Sec. II C) in the low-energy manifold of the 2D model, the calculation can be extended to other low-energy states by working to higher orders in perturbation theory so that all degeneracies are lifted. We expect that our formalism can be applied to the strong leg, left-diagonal, and right-diagonal limits also, providing a large subspace in the parameter space of the coupling constants of the 2D model (see Fig. 7) where the 1D effective theory works. It is also worthwhile to note that the advantage in using the 1D effective model lies in the drastic reduction in the degrees of freedom in certain parameter regimes. It would be interesting to look for other quantum many-body models where this happens.

ACKNOWLEDGMENTS

We acknowledge the use of [QIClib](#) – a modern C++ library for general purpose quantum information processing and quantum computing.

Appendix A: Rotational symmetry of the effective Hamiltonian

In this appendix, we take a slightly more abstract approach and argue that the effective Hamiltonian preserves the rotational symmetry in z direction to any order in perturbation theory in $1/J_{\perp}$. More precisely, writing (note that in this paper we work with only the leading order)

$$\tilde{H} = \sum_{n=0}^{\infty} J_{\perp}^{-n} \tilde{H}^{(n)} \quad (\text{A1})$$

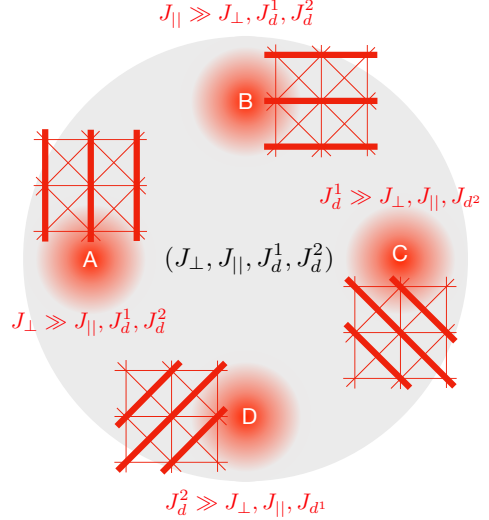


FIG. 7. Schematic representation of the subspaces denoted by (A) $J_{\perp} \gg J_{\parallel}, J_d^1, J_d^2$, (B) $J_{\parallel} \gg J_{\perp}, J_d^1, J_d^2$, (C) $J_d^1 \gg J_{\perp}, J_{\parallel}, J_d^2$, and (D) $J_d^2 \gg J_{\perp}, J_{\parallel}, J_d^1$ in the space of the parameters $J_{\perp}, J_{\parallel}, J_d^1$, and J_d^2 . The thick lines in the lattices represent the strong couplings. While this paper deals with only the subspace (A), the 1D effective model in each of these subspaces can be worked out following the same methodology.

we show below that the $[\tilde{H}^{(n)}, \mathcal{Z}] = 0, \forall n$. The general formalism of perturbation theory provides [98]

$$\begin{aligned} \tilde{H}^{(n)} &= P_g H_0 P_g + P_g H' P_g + P_g H' P_e (P_e H_0 P_e)^{-1} \\ &\times \sum_{n=0}^{\infty} [(P_e H' P_e - EI)(P_e H_0 P_e)^{-1}]^n P_e H' P_g. \end{aligned} \quad (\text{A2})$$

Note that the only operators on the RHS are H' and P_g (recall that P_g are the projector to ground state manifold). The proof that $[\tilde{H}^{(n)}, \mathcal{Z}] = 0$ then follows simply from the fact that $[H', \mathcal{Z}] = 0$ and $[P_g, \mathcal{Z}] = 0$ – the former is simply the consequence of rotational symmetry of the 2D system (Eq. (1)) and the latter we prove below. Note that we can construct P_g explicitly as

$$P_g = \sum_l |\Psi_l\rangle \langle \Psi_l|. \quad (\text{A3})$$

Since from Eq. (19), $|\Psi_l\rangle$ is an eigenvector of the Hermitian operator \mathcal{Z} , it is obvious that $[P_g, \mathcal{Z}] = 0$.

Appendix B: Low-energy effective Hamiltonian for OBC along rungs

In this Section, we present the important steps of determining the effective coupling strengths \tilde{J}_{xy} , \tilde{J}_{zz} , and \tilde{h} in Eq. (21), with $|\psi_0^{(i)}\rangle$ and $|\psi_1^{(i)}\rangle$ given in Eqs. (37) and (46). Similar to Sec. III, we have assumed $J_{\perp} = 1$ for brevity. Also, For ease of reference, we write

$$H' = H_L + H_D + H_F. \quad (\text{B1})$$

Here, H_L is the leg-Hamiltonian given by

$$H_L = \frac{J_{||}}{4} \sum_{i=1}^N \sum_{j=1}^L \vec{\sigma}_{i,j} \cdot \vec{\sigma}_{i+1,j}, \quad (\text{B2})$$

and $H_D = H_{D_L} + H_{D_R}$ represents the diagonal interactions with

$$H_{D_L} = \frac{J_d^1}{4} \sum_{i=1}^N \sum_{j=1}^L \vec{\sigma}_{i,j+1} \cdot \vec{\sigma}_{i+1,j}, \quad (\text{B3})$$

and

$$H_{D_R} = \frac{J_d^2}{4} \sum_{i=1}^N \sum_{j=1}^L \vec{\sigma}_{i,j} \cdot \vec{\sigma}_{i+1,j+1} \quad (\text{B4})$$

representing the *left* and *right* diagonals respectively (see Fig. 1). The field-part H_F of the perturbation Hamiltonian is given by

$$H_F = -\frac{\Delta h}{2} \sum_{i=1}^N \sum_{j=1}^L \sigma_{i,j}^z. \quad (\text{B5})$$

We start with the field-contribution in H' , and write $H_F = \sum_{i=1}^N H_{F_i}$, H_{F_i} being the field-term corresponding to the i th rung. The action of H_{F_i} on the states $|\psi_{0,1}^{(i)}\rangle$ along with the definition of τ_i^z leads to the effective Hamiltonian

$$\tilde{H}_F = -\frac{\Delta h}{2} \left[N(L-1)I + \sum_{i=1}^N \tau_i^z \right], \quad (\text{B6})$$

where I is the identity matrix on the ladder Hilbert space. We next consider the leg-term H_L , and treat the terms corresponding to the xy - and the zz -interactions separately, i.e., $H_L = H_L^{xy} + H_L^{zz}$. In the basis $|\psi_{k_i}^{(i)} \psi_{k_{i+1}}^{(i+1)}\rangle$, action of the i th term of H_L^{xy} provides non-zero values for only $\langle \psi_0^{(i)} \psi_1^{(i+1)} | \dots | \psi_1^{(i)} \psi_0^{(i+1)} \rangle$ and its hermitian conjugate, leading to the effective Hamiltonian

$$\tilde{H}_L^{xy} = \frac{J_{||}}{4} \sum_{i=1}^N (\tau_i^x \tau_{i+1}^x + \tau_i^y \tau_{i+1}^y). \quad (\text{B7})$$

On the other hand, i th term of H_L^{zz} additionally has non-zero values for $\langle \psi_0^{(i)} \psi_0^{(i+1)} | \dots | \psi_0^{(i)} \psi_0^{(i+1)} \rangle$ and $\langle \psi_1^{(i)} \psi_1^{(i+1)} | \dots | \psi_1^{(i)} \psi_1^{(i+1)} \rangle$ also, which leads to

$$\begin{aligned} \tilde{H}_L^{zz} &= \frac{NJ_{||}}{16} [3L - 4 + A_1] I \\ &+ \frac{J_{||}}{8} [L - A_1] \sum_{i=1}^N \tau_i^z \\ &+ \frac{J_{||}}{16} [4 - L + A_1] \sum_{i=1}^N \tau_i^z \tau_{i+1}^z, \end{aligned} \quad (\text{B8})$$

with the constant A_1 given in Eq. (49).

Next, we pick up the diagonal terms H_{D_L} and H_{D_R} in the perturbing Hamiltonian (see Eqs. (B3)-(B4)), and proceed by writing $H_D^{xy} = H_{D_L}^{xy} + H_{D_R}^{xy}$ and $H_D^{zz} = H_{D_L}^{zz} + H_{D_R}^{zz}$.

Calculation similar to the effective Hamiltonian of H_L^{xy} and H_L^{zz} provides

$$\tilde{H}_D^{xy} = \frac{1}{4} A_0 (J_d^1 + J_d^2) \sum_{i=1}^N (\tau_i^x \tau_{i+1}^x + \tau_i^y \tau_{i+1}^y). \quad (\text{B9})$$

and

$$\begin{aligned} \tilde{H}_D^{zz} &= \frac{N}{16} [(L-1 + A_3 + 2A_2)(J_d^1 + J_d^2)] I \\ &+ \frac{1}{8} (L-1 - A_3)(J_d^1 + J_d^2) \sum_{i=1}^N \tau_i^z \\ &+ \frac{1}{16} [(L-1 + A_3 - 2A_2)(J_d^1 + J_d^2)] \sum_{i=1}^N \tau_i^z \tau_{i+1}^z, \end{aligned} \quad (\text{B10})$$

with A_0 , A_2 , and A_3 given by Eqs. (48), (50) and (51) respectively. Therefore, combining Eqs. (B6), (B7), (B8), (B9), and (B10), the effective Hamiltonian

$$\tilde{H} = \tilde{H}_F + \tilde{H}_L^{xy} + \tilde{H}_L^{zz} + \tilde{H}_D^{xy} + \tilde{H}_D^{zz} \quad (\text{B11})$$

turns out to be as given in Eq. (21), with the effective couplings and the additive constant are given in Eqs. (47).

In the following, we include the details of the above mapping in the case of $L = 2$ [71, 72, 87–89, 91], $L = 3$ [86, 91], and $L = 4$, and provide the expressions for \tilde{J}_{xy} , \tilde{J}_{zz} , and \tilde{h} , where J_{\perp} is assumed to be 1.

1. $L = 2$

For $L = 2$ [71, 72, 87–89, 91], The i th rung has doubly degenerate ground states ($d = 2$), given by

$$\begin{aligned} |\psi_0^{(i)}\rangle &= |00\rangle, \\ |\psi_1^{(i)}\rangle &= \frac{1}{\sqrt{2}}(|01\rangle - |10\rangle), \end{aligned} \quad (\text{B12})$$

at $h' = 1$, with the ground-state energy $E_0 = -3 \perp / 4$. The coupling constants in \tilde{H} are given by

$$\tilde{J}_{xy} = [2J_{||} - J_d^1 - J_d^2] / 8, \quad (\text{B13})$$

$$\tilde{J}_{zz} = [2J_{||} + J_d^1 + J_d^2] / 16, \quad (\text{B14})$$

$$\tilde{h} = [2J_{||} - 4\Delta h + J_d^1 + J_d^2] / 8. \quad (\text{B15})$$

where we have used PBC along the legs. Using OBC along the legs changes the 1D LEH to Eq. (44), with \tilde{J}_{xy} , \tilde{J}_{zz} , and \tilde{h} given by Eqs. (B13)-(B15), and

$$\tilde{h}' = -[2J_{||} + J_d^1 + J_d^2] / 16. \quad (\text{B16})$$

2. $L = 3$

For $L = 3$ in Eq. (1) [86, 91],

$$\begin{aligned} |\psi_0^{(i)}\rangle &= |000\rangle, \\ |\psi_1^{(i)}\rangle &= (|001\rangle - 2|010\rangle + |100\rangle) / \sqrt{6}, \end{aligned} \quad (\text{B17})$$

which are degenerate at $h' = 3/2$, with ground state energy $E_0 = -7/4$. The effective coupling constants in Eq. (21) are given by

$$\tilde{J}_{xy} = [3J_{||} - 2(J_d^1 + J_d^2)] / 12, \quad (\text{B18})$$

$$\tilde{J}_{zz} = [9J_{||} + 4(J_d^1 + J_d^2)] / 72, \quad (\text{B19})$$

$$\tilde{h} = [9J_{||} + 11(J_d^1 + J_d^2) - 18\Delta h] / 36. \quad (\text{B20})$$

In the case of OBC along the legs, the effective Hamiltonian is modified to Eq. (44) with

$$\tilde{h}' = -[9J_{||} + 11(J_d^1 + J_d^2)] / 72. \quad (\text{B21})$$

3. $L = 4$

For $L = 4$, the doubly-degenerate ground states at $h' = 1 + 1/\sqrt{2}$ are given by

$$\begin{aligned} |\psi_0\rangle &= |0000\rangle, \\ |\psi_1\rangle &= \left[-|0001\rangle + a|0010\rangle - a|0100\rangle \right. \\ &\quad \left. + |1000\rangle \right] / \sqrt{2 + 2a^2}, \end{aligned} \quad (\text{B22})$$

with $a = 1 + \sqrt{2}$. The effective coupling constants in Eq. (21) are given by

$$\begin{aligned} \tilde{J}_{xy} &= [8J_{||} - (2 + 3\sqrt{2})(J_d^1 + J_d^2)] / 32, \\ \tilde{J}_{zz} &= [12J_{||} + (2\sqrt{2} + 5)(J_d^1 + J_d^2)] / 128, \\ \tilde{h} &= [20J_{||} - 32\Delta h + (2\sqrt{2} + 19)(J_d^1 + J_d^2)] / 64. \end{aligned} \quad (\text{B23})$$

Appendix C: Trace distance

Here we briefly discuss the trace and Bures distance metrics used in this paper for quantifying the distance between density matrices of subsystems of the quantum spin ladder. Given two density operators ρ_1 and ρ_2 defined on a Hilbert space of dimension d , the trace-distance between ρ_1 and ρ_2 is defined as [2]

$$\begin{aligned} d_T(\rho_1, \rho_2) &= \frac{1}{2} \sqrt{(\rho_1 - \rho_2)^\dagger (\rho_1 - \rho_2)} \\ &= \frac{1}{2} \sum_{i=1}^d |\lambda_i|, \end{aligned} \quad (\text{C1})$$

where λ_i are the singular values of the Hermitian matrix $\rho_1 - \rho_2$. Note that $\rho_1 - \rho_2$ is not necessarily positive.

Appendix D: Odd number of spins on a rung with vanishing magnetic field

For ease of presenting the steps of the calculation, we set $j_d^1 = J_d^2 = 0$, and redefine the states in Eqs. (55) and (56) as

$$\begin{aligned} |\psi_0^{(i)}\rangle &= \sum_{\{j\} \in S} a_{\{j\}} |\{j\}\rangle, \\ |\psi_1^{(i)}\rangle &= \sum_{\{j\} \in S} a_{\{j\}} |\{\bar{j}\}\rangle. \end{aligned} \quad (\text{D1})$$

Here, $\{j\} = \{j_1, j_2, \dots, j_l\}$, such that $j_1 < j_2 < \dots < j_{(l-1)} < j_l$, with each $j \in S$ where $S \equiv \{1, 2, \dots, L-1, L\}$. In each of the terms in $|\psi_0^{(i)}\rangle$ ($|\psi_1^{(i)}\rangle$), the indices $\{j\}$ indicate the lattice sites of the spins that are in the state $|1\rangle$ ($|0\rangle$), and $|\{\bar{j}\}\rangle$ is the complement of $|\{j\}\rangle$, such that $|\psi_1^{(i)}\rangle = (\sigma^x)^{\otimes L} |\psi_0^{(i)}\rangle$ (see Eq. (56)). We follow the prescription given in Sec. II B. First, we write the leg term as $H_L = H_L^{xy} + H_L^{zz}$ (see Appendix B), where the action of the i th term in H_L^{xy} , corresponding to the i th rung, on two neighbouring rungs $(i, i+1)$ is given by

$$\begin{aligned} &\langle \psi_1^{(i)} \psi_0^{(i+1)} | H_{L_i}^{xy} | \psi_0^{(i)} \psi_1^{(i+1)} \rangle \\ &= \sum_{\{j\} \in S} \sum_{\{j'\} \in S} \sum_k a_{\{j\}} a_{\{j'\}} a_{\{p\}} a_{\{q\}}, \\ &\langle \psi_0^{(i)} \psi_1^{(i+1)} | H_{L_i}^{xy} | \psi_1^{(i)} \psi_0^{(i+1)} \rangle \\ &= \sum_{\{j\} \in S} \sum_{\{j'\} \in S} \sum_k a_{\{j\}} a_{\{j'\}} a_{\{p\}} a_{\{q\}}, \end{aligned} \quad (\text{D2})$$

with $\{p\} = \{p_1, p_2, \dots, p_l\} \in S_1$, where $S_1 = S \setminus \{k, \{j\}\}$ is the set of all elements in S except k and $\{j\}$. Similarly, $\{q\} = \{q_1, q_2, \dots, q_l\} \in S_2$ with $S_2 = S \setminus \{k, \{j'\}\}$, and $k \in S_3$ with $S_3 = S \setminus \{\{j\}, \{j'\}\}$. The action of $H_{L_i}^{xy}$ on $|\psi_0^{(i)} \psi_0^{(i+1)}\rangle$ and $|\psi_1^{(i)} \psi_1^{(i+1)}\rangle$ takes the system out of the ground state manifold. The effective Hamiltonian due to H_L^{xy} therefore becomes

$$\tilde{H}_L^{xy} = A \frac{J_{||}}{4} \sum_{i=1}^N (\tau_i^x \tau_{i+1}^x + \tau_i^y \tau_{i+1}^y), \quad (\text{D3})$$

where

$$A = \sum_{\{j\} \in S} \sum_{\{j'\} \in S} a_{\{j\}} a_{\{j'\}} a_{\{p\}} a_{\{q\}}. \quad (\text{D4})$$

On the other hand, non-zero matrix elements of $H_{L_i}^{zz}$ corresponding to the neighbouring rungs $(i, i+1)$ are

$$\begin{aligned}
& \langle \psi_0^{(i)} \psi_0^{(i+1)} | H_{L_i}^{zz} | \psi_0^{(i)} \psi_0^{(i+1)} \rangle \\
&= \sum_{\{j\} \in S} \sum_{\{j'\} \in S} [2(n_1 + n_2) - L] a_{\{j\}}^2 a_{\{j'\}}^2, \\
& \langle \psi_0^{(i)} \psi_1^{(i+1)} | H_{L_i}^{zz} | \psi_0^{(i)} \psi_1^{(i+1)} \rangle \\
&= \sum_{\{j\} \in S} \sum_{\{j'\} \in S} [L - 2(n_1 + n_2)] a_{\{j\}}^2 a_{\{j'\}}^2, \\
& \langle \psi_1^{(i)} \psi_0^{(i+1)} | H_{L_i}^{zz} | \psi_1^{(i)} \psi_0^{(i+1)} \rangle \\
&= \sum_{\{j\} \in S} \sum_{\{j'\} \in S} [L - 2(n_1 + n_2)] a_{\{j\}}^2 a_{\{j'\}}^2, \\
& \langle \psi_1^{(i)} \psi_1^{(i+1)} | H_{L_i}^{zz} | \psi_1^{(i)} \psi_1^{(i+1)} \rangle \\
&= \sum_{\{j\} \in S} \sum_{\{j'\} \in S} [2(n_1 + n_2) - L] a_{\{j\}}^2 a_{\{j'\}}^2, \quad (D5)
\end{aligned}$$

where n_1 is the cardinality of $\{j\} \cap \{j'\}$, and n_2 is the cardinality of $(S \setminus \{j\}) \cap (S \setminus \{j'\})$. The effective Hamiltonian due to $H_{L_i}^{zz}$, therefore, is

$$\tilde{H}_L^{zz} = B \frac{J_{||}}{4} \sum_{i=1}^N (\tau_i^z \tau_{i+1}^z), \quad (D6)$$

where

$$B = \sum_{\{j\} \in S} \sum_{\{j'\} \in S} [2(n_1 + n_2) - L] a_{\{j\}}^2 a_{\{j'\}}^2. \quad (D7)$$

The effective Hamiltonian $\tilde{H} = \tilde{H}_L^{xy} + \tilde{H}_L^{zz}$, therefore, takes the form of an 1D XXZ Hamiltonian given by Eq. (57), where the coupling constants \tilde{J}_{xy} and \tilde{J}_{zz} are given by

$$\tilde{J}_{xy} = (J_{||} A_4)/4, \quad \tilde{J}_{zz} = (J_{||} B_4)/4. \quad (D8)$$

We now demonstrate the crucial steps of the calculation in the case of three-leg ladder at $h = 0$. We first write $|\psi_0\rangle$ and $|\psi_1\rangle$ as (see Eq. (D1))

$$\begin{aligned}
|\psi_0\rangle &= (a_1 |100\rangle + a_2 |010\rangle + a_3 |001\rangle), \\
|\psi_1\rangle &= (a_1 |011\rangle + a_2 |101\rangle + a_3 |110\rangle), \quad (D9)
\end{aligned}$$

where $a_1 = a_3 = 1/\sqrt{6}$, and $a_2 = -2/\sqrt{6}$. In this notation, consider the action of H_L^{xy} on one of the terms in $|\psi_0^{(i)} \psi_1^{(i+1)}\rangle$, say, $H_L^{xy}(a_1^2 |100011\rangle)$. Here $i_1 = 1$, $j_1 = 1$, $S \equiv \{1, 2, 3\}$, and $S \setminus \{i_1, j_1\} \equiv 2, 3$, implying $k \in \{2, 3\}$. For $k = 2$, $p_1 = S \setminus \{k, i_1\} = 3$, $q_1 = S \setminus \{k, j_1\} = 3$, and for $k = 3$, $p_1 = S \setminus \{k, i_1\} = 2$, $q_1 = S \setminus \{k, j_1\} = 2$. This leads to

$$\begin{aligned}
& \langle \psi_0^{(i)} \psi_1^{(i+1)} | H_L^{xy} (a_1^2 |100011\rangle) \\
&= \sum_k a_{i_1} a_{j_1} a_{p_1} a_{q_1} = a_1^2 a_2^2 + a_1^2 a_3^2. \quad (D10)
\end{aligned}$$

Proceeding in the same way for other terms in $|\psi_0^{(i)} \psi_1^{(i+1)}\rangle$, as well as the other elements of the basis

$$\{|\psi_0^{(i)} \psi_0^{(i+1)}\rangle, |\psi_0^{(i)} \psi_1^{(i+1)}\rangle, |\psi_1^{(i)} \psi_0^{(i+1)}\rangle, |\psi_1^{(i)} \psi_1^{(i+1)}\rangle\}, \quad (D11)$$

and substituting values of a_1, a_2, a_3 , we obtain

$$\begin{aligned}
\langle \psi_1^{(i)} \psi_0^{(i+1)} | H_L^{xy} | \psi_0^{(i)} \psi_1^{(i+1)} \rangle &= 1, \\
\langle \psi_0^{(i)} \psi_1^{(i+1)} | H_L^{xy} | \psi_1^{(i)} \psi_0^{(i+1)} \rangle &= 1, \quad (D12)
\end{aligned}$$

while the other matrix elements vanish.

To see the action of H_L^{zz} on a pair of neighbouring rungs $(i, i+1)$, first consider the action of H_L^{zz} on one of the terms of in $|\psi_0^{(i)} \psi_0^{(i+1)}\rangle$, say $H_L^{zz}(a_1 a_2 |100010\rangle)$. To determine the contribution of this term to $\langle \psi_0^{(i)} \psi_0^{(i+1)} | H_L^{zz} | \psi_0^{(i)} \psi_0^{(i+1)} \rangle$, note that $i_1 = 1$, $j_1 = 2$, $\mathcal{I} \equiv \{1\}$, and $\mathcal{J} \equiv \{2\}$, which leads to $n_1 = 0$, and $n_2 = 1$. Therefore, for $i_1 = 1$ and $j_1 = 2$, $n_1 + n_2 - (L - n_1 - n_2) = -1$. Using the same procedure for other terms in $|\psi_0^{(i)} \psi_0^{(i+1)}\rangle$ as well as the other elements of the basis, and substituting values for a_1, a_2 and a_3 , we obtain non-zero matrix elements of H_L^{zz} as

$$\begin{aligned}
\langle \psi_0^{(i)} \psi_0^{(i+1)} | H_L^{zz} | \psi_0^{(i)} \psi_0^{(i+1)} \rangle &= 1 \\
\langle \psi_0^{(i)} \psi_1^{(i+1)} | H_L^{zz} | \psi_0^{(i)} \psi_1^{(i+1)} \rangle &= -1 \\
\langle \psi_1^{(i)} \psi_0^{(i+1)} | H_L^{zz} | \psi_1^{(i)} \psi_0^{(i+1)} \rangle &= -1 \\
\langle \psi_1^{(i)} \psi_1^{(i+1)} | H_L^{zz} | \psi_1^{(i)} \psi_1^{(i+1)} \rangle &= 1. \quad (D13)
\end{aligned}$$

This leads to $A_4 = 1 = B_4 = 1$ (see Eqs. (D4) and (D7)). Therefore, the coefficients of the 1D LEH (Eq. (57)), given by Eq. (D8), are

$$\tilde{J}_{xy} = (J_{||})/4, \quad \tilde{J}_{zz} = (J_{||})/4. \quad (D14)$$

We point out here that the coupling constants can also be determined in a similar fashion with perturbations $J_d^1, J_d^2 \neq 0$, where the overall form of Eq. (57) remains unchanged.

Appendix E: Entanglement and related measures of quantum correlations

In this section, we provide brief definitions of the quantum correlation measures investigated in the quantum spin ladder. More specifically, we focus on bipartite entanglement [25, 26] between different parts of the system, as quantified by negativity [25, 118–123], and multipartite quantum correlation over the complete system, or a chosen subsystem, as quantified by the entanglement monogamy score [112, 113, 115].

1. Negativity

Entanglement between two partitions A and B of a bipartite quantum state ρ_{AB} is quantified by a bipartite entanglement measure [25, 26], such as the negativity [118–124]. It is defined as

$$E_{S;\bar{S}} = \|\rho_{S\bar{S}}^{T_{\bar{S}}}\| - 1, \quad (E1)$$

with $\|\varrho\| = \text{Tr} \sqrt{\varrho^\dagger \varrho}$ being the trace norm of ϱ (see also Appendix C), and $\rho_{S\bar{S}}^{T_{\bar{S}}}$ is obtained by performing partial transposition of the density matrix $\rho_{S\bar{S}}$ with respect to the subsystem \bar{S} .

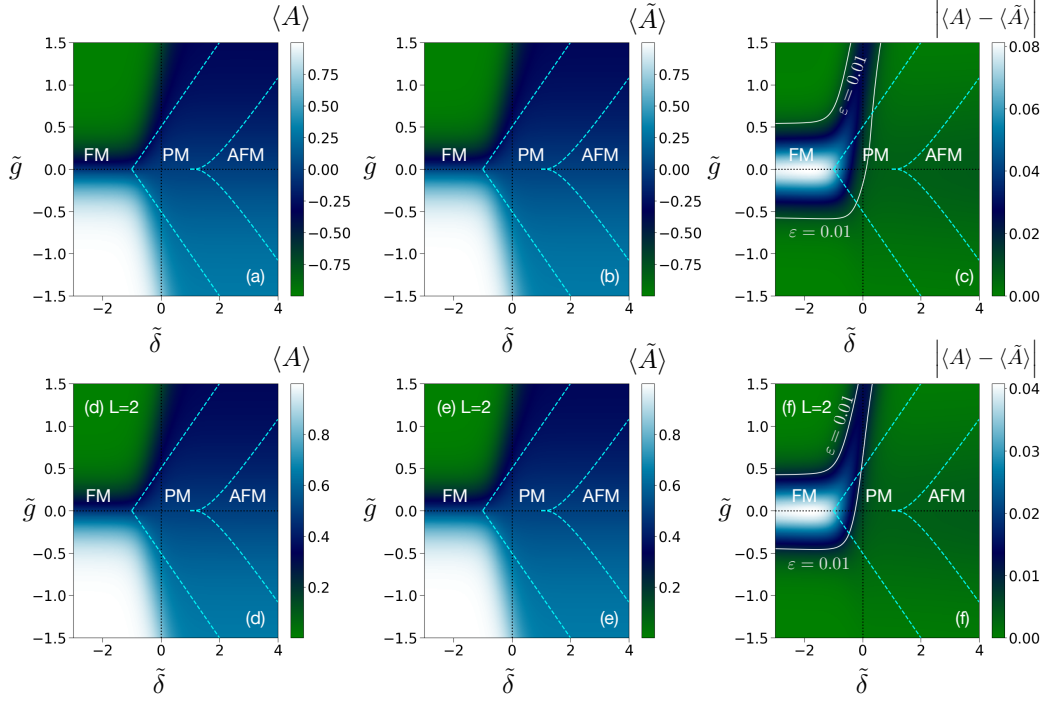


FIG. 8. Variations of $\langle A \rangle$, $\langle \tilde{A} \rangle$, and $\varepsilon = \langle A \rangle - \langle \tilde{A} \rangle$ as functions of $\tilde{\delta}$ and \tilde{g} for a 3×2 lattice, where $A = \sigma_{i,1}^z \otimes \sigma_{i,2}^z$ (plotted in (a)), and $A = \sigma_{i,1}^z$ (plotted in (d)). The corresponding low-energy operators are $\tilde{A} = \tau_i^z$ (plotted in (b)) and $\tilde{A} = (I_i + \tau_i^z)/2$ (plotted in (e)) respectively (see Table I). All quantities plotted are dimensionless.

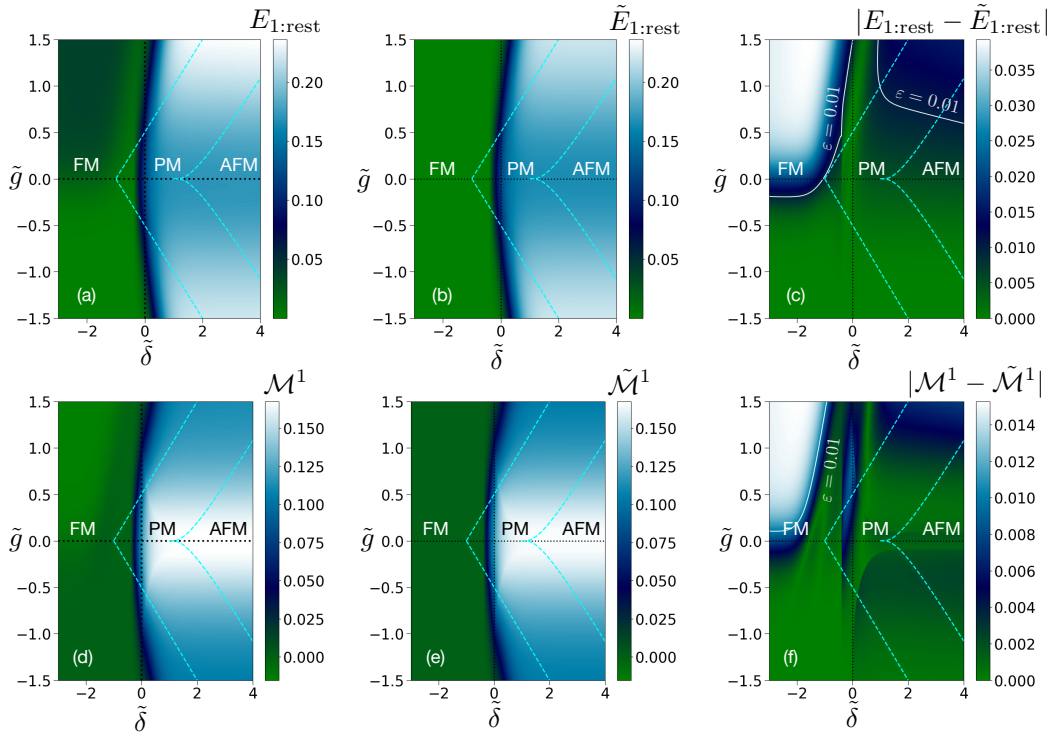


FIG. 9. Variations of (a) $E_{1,\text{rest}}$, (b) $\tilde{E}_{1,\text{rest}}$, (c) $\varepsilon = |E_{1,\text{rest}} - \tilde{E}_{1,\text{rest}}|$, (d) \mathcal{M}^1 , (e) $\tilde{\mathcal{M}}^1$, and (f) $\varepsilon = |\mathcal{M}^1 - \tilde{\mathcal{M}}^1|$ as functions of $\tilde{\delta}$ and \tilde{g} for a 3×2 lattice. The continuous lines signify the value 10^{-2} for the respective quantities. All quantities plotted are dimensionless.

2. Monogamy of entanglement

For a given bipartite entanglement measure E and an N -party quantum state $\rho_{S_1 S_2 \dots S_N}$, the quantum state is said to be *monogamous* [110–114, 117] for the entanglement measure E if

$$E_{S_i:\text{rest}} \geq \sum_{i \neq j} E_{S_i S_j} \quad (\text{E2})$$

for $i, j \in \{1, 2, \dots, N\}$ with S_i as the *nodal observer*, where $E_{S_i:\text{rest}} = E(\rho_{S_i:\text{rest}})$ computed over the bipartition $S_i : \text{rest}$ of the N -party system, and $E_{S_i S_j} = E(\rho_{S_i S_j})$ with $\rho_{S_i S_j} = \text{Tr}_{\{S_k; k \neq i, j\}}[\rho_{S_1 S_2 \dots S_N}]$. The corresponding monogamy score [115, 117] is defined as

$$\mathcal{M}^{S_i} = E_{S_i:\text{rest}} - \sum_{i \neq j} E_{S_i S_j}, \quad (\text{E3})$$

where a positive (negative) value of \mathcal{M}^{S_i} indicates that the state $\rho_{S_1 S_2 \dots S_N}$ is monogamous (non-monogamous) for the bipartite entanglement measure E with S_i as the node. Entanglement monogamy score captures multiparty quantum correlation present in the N -party system [116].

Appendix F: Expectation values of observables on a rung

Here we briefly discuss the variations of the expectation values of $A = \sigma_{i,1}^z$ and $A = \sigma_{i,1}^z \otimes \sigma_{i,2}^z$ on the i th rung of a 3×2 lattice, and their corresponding low-energy components \tilde{A} , as functions of $\tilde{\delta}$ and \tilde{g} (see Fig. 8). Note that in the strong rung-coupling limit, a rung is mapped to an effective two-level system constituting the 1D effective XXZ model. Therefore, we expect $A = \sigma_{i,j}^z$ and $A = \sigma_{i,1}^z \otimes \sigma_{i,2}^z$

to qualitatively have similar behaviour as functions of system parameters. This is confirmed by Figs. 8(a) and (d). The low-energy components of $A = \sigma_{i,1}^z \otimes \sigma_{i,2}^z$ and $A = \sigma_{i,j}^z$ are given by $\tilde{A} = \tau_i^z$ and $\tilde{A} = (I_i + \tau_i^z)/2$ respectively, and $\langle \tilde{A} \rangle$ in $\tilde{\rho}$ also match for these two observables over the entire $(\tilde{\delta}, \tilde{g})$ plane. Moreover, $\varepsilon = |\langle A \rangle - \langle \tilde{A} \rangle|$ also match for both observables.

Appendix G: Bipartite entanglement and entanglement monogamy score

We now discuss two specific types of quantum correlations on a 3×2 lattice – (a) the bipartite entanglement, $E_{1:\text{rest}}$, as quantified by negativity (see Appendix E), between the rung $i = 1$ and the rest of the system, and (b) the entanglement monogamy score \mathcal{M}^1 on the lattice, taking one of the rungs, say, rung $i = 1$, as the nodal observer. Correspondingly, in the 1D effective XXZ model, we compute (a) the bipartite entanglement $\tilde{E}_{1:\text{rest}}$ between the spin $i = 1$ and the rest of the system, and (b) the entanglement monogamy score $\tilde{\mathcal{M}}^1$ over the 3-spin effective model using the spin $i = 1$ as the nodal observer. Fig. 9 depicts the variations of these quantum correlations as functions of $\tilde{\delta}$ and \tilde{g} . Similar to the case of $E_{i,i+1}$ and $\tilde{E}_{i,i+1}$ as described in Sec. V, the qualitative variations of these quantum correlations in the 2D model and their counterparts in the 1D effective XXZ model are found to be matching. Moreover, the plots of $\varepsilon = |E_{1:\text{rest}} - \tilde{E}_{1:\text{rest}}|$ and $\varepsilon = |\mathcal{M}^1 - \tilde{\mathcal{M}}^1|$ as functions of $(\tilde{\delta}, \tilde{g})$ are also qualitatively similar, with relatively high value of ε found in the FM phase with positive magnetic field. These observations are in agreement with the ones made in the case of nearest-neighbor entanglement in the 2D and the effective 1D model in Sec. V.

-
- [1] M. A. Nielsen and I. L. Chuang, *Quantum Computation and Quantum Information* (Cambridge University Press, 2010).
- [2] M. M. Wilde, *Quantum Information Theory, 2nd ed.* (Cambridge University Press, Cambridge, UK, 2017).
- [3] Indrani Bose, “Low-dimensional quantum spin systems,” in *Field Theories in Condensed Matter Physics* (Hindustan Book Agency, Gurgaon, 2001) pp. 359–408.
- [4] Alexander Vasiliev, Olga Volkova, Elena Zvereva, and Maria Markina, “Milestones of low-d quantum magnetism,” *npg Quantum Materials* **3**, 18 (2018).
- [5] Luigi Amico, Rosario Fazio, Andreas Osterloh, and Vlatko Vedral, “Entanglement in many-body systems,” *Rev. Mod. Phys.* **80**, 517–576 (2008).
- [6] J I Latorre and A Riera, “A short review on entanglement in quantum spin systems,” *Journal of Physics A: Mathematical and Theoretical* **42**, 504002 (2009).
- [7] Kavan Modi, Aharon Brodutch, Hugo Cable, Tomasz Paterek, and Vlatko Vedral, “The classical-quantum boundary for correlations: Discord and related measures,” *Rev. Mod. Phys.* **84**, 1655–1707 (2012).
- [8] Nicolas Laflorencie, “Quantum entanglement in condensed matter systems,” *Physics Reports* **646**, 1–59 (2016), quantum entanglement in condensed matter systems.
- [9] Gabriele De Chiara and Anna Sanpera, “Genuine quantum correlations in quantum many-body systems: a review of recent progress,” *Reports on Progress in Physics* **81**, 074002 (2018).
- [10] Anindita Bera, Tamoghna Das, Debasis Sadhukhan, Sudipto Singha Roy, Aditi Sen(De), and Ujjwal Sen, “Quantum discord and its allies: a review of recent progress,” *Reports on Progress in Physics* **81**, 024001 (2017).
- [11] Sougato Bose, “Quantum communication through an unmodulated spin chain,” *Phys. Rev. Lett.* **91**, 207901 (2003).
- [12] Daniel Burgarth and Sougato Bose, “Conclusive and arbitrarily perfect quantum-state transfer using parallel spin-chain channels,” *Phys. Rev. A* **71**, 052315 (2005).
- [13] Daniel Burgarth, Vittorio Giovannetti, and Sougato Bose, “Efficient and perfect state transfer in quantum chains,” *Journal of Physics A: Mathematical and General* **38**, 6793 (2005).
- [14] Daniel Burgarth and Sougato Bose, “Perfect quantum state transfer with randomly coupled quantum chains,” *New Journal of Physics* **7**, 135 (2005).
- [15] B Vaucher, D Burgarth, and S Bose, “Arbitrarily perfect quantum communication using unmodulated spin chains, a

- collaborative approach,” *Journal of Optics B: Quantum and Semiclassical Optics* **7**, S356 (2005).
- [16] Sougato Bose, Abolfazl Bayat, Pasquale Sodano, Leonardo Banchi, and Paola Verrucchi, “Spin chains as data buses, logic buses and entanglers,” in *Quantum State Transfer and Network Engineering*, edited by Georgios M. Nikolopoulos and Igor Jex (Springer Berlin, Heidelberg, 2013) Chap. 1, pp. 1–38.
- [17] Robert Raussendorf and Hans J. Briegel, “A one-way quantum computer,” *Phys. Rev. Lett.* **86**, 5188–5191 (2001).
- [18] Robert Raussendorf, Daniel E. Browne, and Hans J. Briegel, “Measurement-based quantum computation on cluster states,” *Phys. Rev. A* **68**, 022312 (2003).
- [19] H. J. Briegel, D. E. Browne, W. Dür, R. Raussendorf, and M. Van den Nest, “Measurement-based quantum computation,” *Nat. Phys.* **5**, 19 (2009).
- [20] Tzu-Chieh Wei, “Quantum spin models for measurement-based quantum computation,” *Advances in Physics: X* **3**, 1461026 (2018).
- [21] Eric Dennis, Alexei Kitaev, Andrew Landahl, and John Preskill, “Topological quantum memory,” *J. Math. Phys.* **43**, 4452–4505 (2002).
- [22] Alexei Kitaev, “Anyons in an exactly solved model and beyond,” *Ann. Phys.* **321**, 2 – 111 (2006).
- [23] H. Bombin and M. A. Martin-Delgado, “Topological quantum distillation,” *Phys. Rev. Lett.* **97**, 180501 (2006).
- [24] H. Bombin and M. A. Martin-Delgado, “Topological computation without braiding,” *Phys. Rev. Lett.* **98**, 160502 (2007).
- [25] Ryszard Horodecki, Paweł Horodecki, Michał Horodecki, and Karol Horodecki, “Quantum entanglement,” *Rev. Mod. Phys.* **81**, 865–942 (2009).
- [26] Otfried Gühne and Géza Tóth, “Entanglement detection,” *Phys. Rep.* **474**, 1–75 (2009).
- [27] U. Schollwöck, “The density-matrix renormalization group,” *Rev. Mod. Phys.* **77**, 259–315 (2005).
- [28] F. Verstraete, V. Murg, and J.I. Cirac, “Matrix product states, projected entangled pair states, and variational renormalization group methods for quantum spin systems,” *Advances in Physics* **57**, 143–224 (2008).
- [29] Ulrich Schollwöck, “The density-matrix renormalization group in the age of matrix product states,” *Annals of Physics* **326**, 96–192 (2011), January 2011 Special Issue.
- [30] Román Orús, “A practical introduction to tensor networks: Matrix product states and projected entangled pair states,” *Annals of Physics* **349**, 117–158 (2014).
- [31] Jacob C Bridgeman and Christopher T Chubb, “Hand-waving and interpretive dance: an introductory course on tensor networks,” *Journal of Physics A: Mathematical and Theoretical* **50**, 223001 (2017).
- [32] F. Verstraete and J. I. Cirac, “Renormalization algorithms for quantum-many body systems in two and higher dimensions,” *arXiv:cond-mat/0407066* (2004).
- [33] G. Vidal, “Entanglement renormalization,” *Phys. Rev. Lett.* **99**, 220405 (2007).
- [34] G. Vidal, “Class of quantum many-body states that can be efficiently simulated,” *Phys. Rev. Lett.* **101**, 110501 (2008).
- [35] Matteo Rizzi, Simone Montangero, and Guifré Vidal, “Simulation of time evolution with multiscale entanglement renormalization ansatz,” *Phys. Rev. A* **77**, 052328 (2008).
- [36] Miguel Aguado and Guifré Vidal, “Entanglement renormalization and topological order,” *Phys. Rev. Lett.* **100**, 070404 (2008).
- [37] Lukasz Cincio, Jacek Dziarmaga, and Marek M. Rams, “Multiscale entanglement renormalization ansatz in two dimensions: Quantum ising model,” *Phys. Rev. Lett.* **100**, 240603 (2008).
- [38] G. Evenbly and G. Vidal, “Algorithms for entanglement renormalization,” *Phys. Rev. B* **79**, 144108 (2009).
- [39] D. Porras and J. I. Cirac, “Effective quantum spin systems with trapped ions,” *Phys. Rev. Lett.* **92**, 207901 (2004).
- [40] D. Leibfried, E. Knill, S. Seidelin, J. Britton, R. B. Blakestad, J. Chiaverini, D. B. Hume, W. M. Itano, J. D. Jost, C. Langer, R. Ozeri, R. Reichle, and D. J. Wineland, “Creation of a six-atom ‘schrodinger cat’ state,” *Nature* **438**, 639–642 (2005).
- [41] Thomas Monz, Philipp Schindler, Julio T. Barreiro, Michael Chwalla, Daniel Nigg, William A. Coish, Maximilian Harlander, Wolfgang Hänsel, Markus Hennrich, and Rainer Blatt, “14-qubit entanglement: Creation and coherence,” *Phys. Rev. Lett.* **106**, 130506 (2011).
- [42] S Korenblit, D Kafri, W C Campbell, R Islam, E E Edwards, Z-X Gong, G-D Lin, L-M Duan, J Kim, K Kim, and C Monroe, “Quantum simulation of spin models on an arbitrary lattice with trapped ions,” *New Journal of Physics* **14**, 095024 (2012).
- [43] Justin G. Bohnet, Brian C. Sawyer, Joseph W. Britton, Michael L. Wall, Ana Maria Rey, Michael Foss-Feig, and John J. Bollinger, “Quantum spin dynamics and entanglement generation with hundreds of trapped ions,” *Science* **352**, 1297–1301 (2016), <https://www.science.org/doi/pdf/10.1126/science.aad9958>.
- [44] R. Barends, J. Kelly, A. Megrant, A. Veitia, D. Sank, E. Jeffrey, T. C. White, J. Mutus, A. G. Fowler, B. Campbell, Y. Chen, Z. Chen, B. Chiaro, A. Dunsworth, C. Neill, P. O’Malley, P. Roushan, A. Vainsencher, J. Wenner, A. N. Korotkov, A. N. Cleland, and John M. Martinis, “Superconducting quantum circuits at the surface code threshold for fault tolerance,” *Nature* **508**, 500 (2014).
- [45] Yariv Yanay, Jochen Braumüller, Simon Gustavsson, William D. Oliver, and Charles Tahan, “Two-dimensional hard-core bose-hubbard model with superconducting qubits,” *npj Quantum Information* **6**, 58 (2020).
- [46] L. M. K. Vandersypen and I. L. Chuang, “Nmr techniques for quantum control and computation,” *Rev. Mod. Phys.* **76**, 1037–1069 (2005).
- [47] C. Negrevergne, T. S. Mahesh, C. A. Ryan, M. Ditty, F. Cyr-Racine, W. Power, N. Boulant, T. Havel, D. G. Cory, and R. Laflamme, “Benchmarking quantum control methods on a 12-qubit system,” *Phys. Rev. Lett.* **96**, 170501 (2006).
- [48] M. Schechter and P. C. E. Stamp, “Derivation of the low- t phase diagram of $\text{LiHo}_x\text{Y}_{1-x}\text{F}_4$: A dipolar quantum ising magnet,” *Phys. Rev. B* **78**, 054438 (2008).
- [49] C. E. Bradley, J. Randall, M. H. Abobeih, R. C. Berrevoets, M. J. Degen, M. A. Bakker, M. Markham, D. J. Twitchen, and T. H. Taminiau, “A ten-qubit solid-state spin register with quantum memory up to one minute,” *Phys. Rev. X* **9**, 031045 (2019).
- [50] Markus Greiner, Olaf Mandel, Tilman Esslinger, Theodor W. Hänsch, and Immanuel Bloch, “Quantum phase transition from a superfluid to a mott insulator in a gas of ultracold atoms,” *Nature* **415**, 39–44 (2002).
- [51] L.-M. Duan, E. Demler, and M. D. Lukin, “Controlling spin exchange interactions of ultracold atoms in optical lattices,” *Phys. Rev. Lett.* **91**, 090402 (2003).
- [52] Immanuel Bloch, “Exploring quantum matter with ultracold atoms in optical lattices,” *Journal of Physics B: Atomic, Molecular and Optical Physics* **38**, S629 (2005).
- [53] Immanuel Bloch, Jean Dalibard, and Wilhelm Zwerger, “Many-body physics with ultracold gases,” *Rev. Mod. Phys.*

- 80**, 885–964 (2008).
- [54] J. Struck, M. Weinberg, C. Ölschläger, P. Windpassinger, J. Simonet, K. Sengstock, R. Höppner, P. Hauke, A. Eckardt, M. Lewenstein, and L. Mathey, “Engineering ising-xy spin-models in a triangular lattice using tunable artificial gauge fields,” *Nature Physics* **9**, 738–743 (2013).
- [55] W. Heisenberg, “Zur theorie des ferromagnetismus,” *Zeitschrift für Physik* **49**, 619–636 (1928).
- [56] Yukio Okwamoto, “Phase diagram of a two-dimensional heisenberg antiferromagnet in a magnetic field,” *Journal of the Physical Society of Japan* **53**, 2434–2436 (1984).
- [57] S. S. Aplesnin, “Quantum monte carlo investigation of the 2d heisenberg model with $s=1/2$,” *Physics of the Solid State* **41**, 103–107 (1999).
- [58] Zheng Weihong, Ross H. McKenzie, and Rajiv R. P. Singh, “Phase diagram for a class of spin- $\frac{1}{2}$ heisenberg models interpolating between the square-lattice, the triangular-lattice, and the linear-chain limits,” *Phys. Rev. B* **59**, 14367–14375 (1999).
- [59] B.V. Costa and A.S.T. Pires, “Phase diagrams of a two-dimensional heisenberg antiferromagnet with single-ion anisotropy,” *Journal of Magnetism and Magnetic Materials* **262**, 316–324 (2003).
- [60] Alessandro Cuccoli, Giacomo Gori, Ruggero Vaia, and Paola Verrucchi, “Phase diagram of the two-dimensional quantum antiferromagnet in a magnetic field,” *Journal of Applied Physics* **99**, 08H503 (2006).
- [61] Hyejin Ju, Ann B. Kallin, Paul Fendley, Matthew B. Hastings, and Roger G. Melko, “Entanglement scaling in two-dimensional gapless systems,” *Phys. Rev. B* **85**, 165121 (2012).
- [62] Ruben Verresen, Frank Pollmann, and Roderich Moessner, “Quantum dynamics of the square-lattice heisenberg model,” *Phys. Rev. B* **98**, 155102 (2018).
- [63] Ozan S. Sarıyer, “Two-dimensional quantum-spin-1/2 xxz magnet in zero magnetic field: Global thermodynamics from renormalisation group theory,” *Philosophical Magazine* **99**, 1787–1824 (2019).
- [64] Zheng Weihong, Ross H. McKenzie, and Rajiv R. P. Singh, “Phase diagram for a class of spin- $\frac{1}{2}$ heisenberg models interpolating between the square-lattice, the triangular-lattice, and the linear-chain limits,” *Phys. Rev. B* **59**, 14367–14375 (1999).
- [65] Ann B. Kallin, Matthew B. Hastings, Roger G. Melko, and Rajiv R. P. Singh, “Anomalies in the entanglement properties of the square-lattice heisenberg model,” *Phys. Rev. B* **84**, 165134 (2011).
- [66] H. Francis Song, Nicolas Laflorencie, Stephan Rachel, and Karyn Le Hur, “Entanglement entropy of the two-dimensional heisenberg antiferromagnet,” *Phys. Rev. B* **83**, 224410 (2011).
- [67] L.S. Lima, “Entanglement and quantum phase transition in the anisotropic two-dimensional xxz model,” *Solid State Communications* **309**, 113836 (2020).
- [68] Elisa Ercolessi, “One and quasi-one dimensional spin systems,” *Modern Physics Letters A* **18**, 2329–2336 (2003).
- [69] N Ivanov, “Spin models of quasi-1d quantum ferrimagnets with competing interactions,” [arXiv:0909.2182](https://arxiv.org/abs/0909.2182) (2009), 10.48550/arXiv.0909.2182.
- [70] Elbio Dagotto and T. M. Rice, “Surprises on the way from one- to two-dimensional quantum magnets: The ladder materials,” *Science* **271**, 618–623 (1996), <https://www.science.org/doi/pdf/10.1126/science.271.5249.618>.
- [71] M T Batchelor, X-W Guan, A Foerster, and H-Q Zhou, “Note on the thermodynamic bethe ansatz approach to the quantum phase diagram of the strong coupling ladder compounds,” *New Journal of Physics* **5**, 107–107 (2003).
- [72] M.T. Batchelor, X.-W. Guan, A. Foerster, A.P. Tonel, and H.-Q. Zhou, “Thermodynamic properties of an integrable quantum spin ladder with boundary impurities,” *Nuclear Physics B* **669**, 385–416 (2003).
- [73] M. T. Batchelor, X. W. Guan, N. Oelkers, and Z. Tsuboi, “Integrable models and quantum spin ladders: Comparison between theory and experiment for the strong coupling ladder compounds,” *Advances in Physics* **56**, 465–543 (2007).
- [74] Ying Li, Tao Shi, Bing Chen, Zhi Song, and Chang-Pu Sun, “Quantum-state transmission via a spin ladder as a robust data bus,” *Phys. Rev. A* **71**, 022301 (2005).
- [75] Guilherme M.A. Almeida, Andre M.C. Souza, Francisco A.B.F. de Moura, and Marcelo L. Lyra, “Robust entanglement transfer through a disordered qubit ladder,” *Physics Letters A* **383**, 125847 (2019).
- [76] Jun-Liang Song, Shi-Jian Gu, and Hai-Qing Lin, “Quantum entanglement in the $s = 1/2$ spin ladder with ring exchange,” *Phys. Rev. B* **74**, 155119 (2006).
- [77] Yan Chen, Paolo Zanardi, Z D Wang, and F C Zhang, “Sublattice entanglement and quantum phase transitions in antiferromagnetic spin chains,” *New Journal of Physics* **8**, 97 (2006).
- [78] Himadri Shekhar Dhar and Aditi Sen(De), “Entanglement in resonating valence bond states: ladder versus isotropic lattices,” *Journal of Physics A: Mathematical and Theoretical* **44**, 465302 (2011).
- [79] JIE REN and SHIQUN ZHU, “Fidelity and entanglement close to quantum phase transition in a two-leg xxz spin ladder,” *International Journal of Quantum Information* **09**, 531–537 (2011).
- [80] Andreas M. Läuchli and John Schliemann, “Entanglement spectra of coupled $s = \frac{1}{2}$ spin chains in a ladder geometry,” *Phys. Rev. B* **85**, 054403 (2012).
- [81] Himadri Shekhar Dhar, Aditi Sen(De), and Ujjwal Sen, “The density matrix recursion method: genuine multisite entanglement distinguishes odd from even quantum spin ladder states,” *New Journal of Physics* **15**, 013043 (2013).
- [82] Raul A. Santos, Chao-Ming Jian, and Rex Lundgren, “Bulk entanglement spectrum in gapped spin ladders,” *Phys. Rev. B* **93**, 245101 (2016).
- [83] Sudipto Singha Roy, Himadri Shekhar Dhar, Debraj Rakshit, Aditi Sen(De), and Ujjwal Sen, “Detecting phase boundaries of quantum spin-1/2 xxz ladder via bipartite and multipartite entanglement transitions,” *Journal of Magnetism and Magnetic Materials* **444**, 227–235 (2017).
- [84] Sheng-Hao Li, Qian-Qian Shi, Murray T Batchelor, and Huan-Qiang Zhou, “Groundstate fidelity phase diagram of the fully anisotropic two-leg spin- $\frac{1}{2}$ xxz ladder,” *New Journal of Physics* **19**, 113027 (2017).
- [85] John Schliemann and Andreas M Läuchli, “Entanglement spectra of heisenberg ladders of higher spin,” *Journal of Statistical Mechanics: Theory and Experiment* **2012**, P11021 (2012).
- [86] Kenro Kawano and Minoru Takahashi, “Three-leg antiferromagnetic heisenberg ladder with frustrated boundary condition; ground state properties,” *Journal of the Physical Society of Japan* **66**, 4001–4008 (1997).
- [87] Keisuke Totsuka, “Magnetization plateau in the $s = \frac{1}{2}$ heisenberg spin chain with next-nearest-neighbor and alternating nearest-neighbor interactions,” *Phys. Rev. B* **57**, 3454–

- 3465 (1998).
- [88] Takashi Tonegawa, Takeshi Nishida, and Makoto Kaburagi, “Ground-state magnetization curve of a generalized spin-1/2 ladder,” *Physica B: Condensed Matter* **246-247**, 368–371 (1998).
- [89] F. Mila, “Ladders in a magnetic field: A strong coupling approach,” *The European Physical Journal B - Condensed Matter and Complex Systems* **6**, 201–205 (1998).
- [90] G. Chaboussant, M. H. Julien, Y. Fagot-Revurat, M. Hanson, L. P. Lévy, C. Berthier, M. Horvatic, and O. Piovesana, “Zero temperature phase transitions in spin-ladders: Phase diagram and dynamical studies of $\text{Cu}_2(\text{C}_5\text{H}_{12}\text{N}_2)_2\text{Cl}_4$,” *The European Physical Journal B - Condensed Matter and Complex Systems* **6**, 167–181 (1998).
- [91] Kunj Tandon, Siddhartha Lal, Swapan K. Pati, S. Ramasesha, and Diptiman Sen, “Magnetization properties of some quantum spin ladders,” *Phys. Rev. B* **59**, 396–410 (1999).
- [92] Michael E. Fisher, “Magnetism in one-dimensional systems—the heisenberg model for infinite spin,” *American Journal of Physics* **32**, 343–346 (1964).
- [93] T. Giamarchi, *Quantum physics in one dimension*, International series of monographs on physics (Clarendon Press, Oxford, 2004).
- [94] Frédéric Mila, “Quantum spin liquids,” *European Journal of Physics* **21**, 499–510 (2000).
- [95] F. Franchini, *An Introduction to Integrable Techniques for One-Dimensional Quantum Systems*, Lecture Notes in Physics (Springer Cham, Switzerland, 2017).
- [96] Amit Tribedi and Indrani Bose, “Spin- $\frac{1}{2}$ heisenberg ladder: Variation of entanglement and fidelity measures close to quantum critical points,” *Phys. Rev. A* **79**, 012331 (2009).
- [97] S. Chen, L. Wang, and Y. P. Wang, “Phase diagram of frustrated mixed-spin ladders in the strong-coupling limit,” *The European Physical Journal B* **57**, 265–270 (2007).
- [98] Frédéric Mila and Kai Phillip Schmidt, “Strong-coupling expansion and effective hamiltonians,” in *Introduction to Frustrated Magnetism: Materials, Experiments, Theory*, edited by Claudine Lacroix, Philippe Mendels, and Frédéric Mila (Springer Berlin Heidelberg, Berlin, Heidelberg, 2011) pp. 537–559.
- [99] D. M. Greenberger, M. A. Horne, and A. Zeilinger, *Bell’s theorem, quantum theory and conceptions of the universe* (Kluwer, Netherlands, 1989).
- [100] A. Zeilinger, M. A. Horne, and D. M. Greenberger, “Higher-order quantum entanglement,” in *Proceedings of Squeezed States and Quantum Uncertainty*, Vol. 73 (NASA Conf. Publ, 1992) p. 3135.
- [101] Elliott Lieb, Theodore Schultz, and Daniel Mattis, “Two soluble models of an antiferromagnetic chain,” *Annals of Physics* **16**, 407–466 (1961).
- [102] Eytan Barouch, Barry M. McCoy, and Max Dresden, “Statistical mechanics of the XY model. i,” *Phys. Rev. A* **2**, 1075–1092 (1970).
- [103] Eytan Barouch and Barry M. McCoy, “Statistical mechanics of the xy model. ii. spin-correlation functions,” *Phys. Rev. A* **3**, 786–804 (1971).
- [104] Eytan Barouch and Barry M. McCoy, “Statistical mechanics of the XY model. iii,” *Phys. Rev. A* **3**, 2137–2140 (1971).
- [105] Hans-Jürgen Mikeska and Alexei K. Kolezhuk, “One-dimensional magnetism,” in *Quantum Magnetism*, edited by Ulrich Schollwöck, Johannes Richter, Damian J. J. Farnell, and Raymond F. Bishop (Springer Berlin Heidelberg, Berlin, Heidelberg, 2004) pp. 1–83.
- [106] Hui Li and F. D. M. Haldane, “Entanglement spectrum as a generalization of entanglement entropy: Identification of topological order in non-abelian fractional quantum hall effect states,” *Phys. Rev. Lett.* **101**, 010504 (2008).
- [107] Tzu-Chieh Wei, Dyutiman Das, Swagatam Mukhopadhyay, Smitha Vishveshwara, and Paul M. Goldbart, “Global entanglement and quantum criticality in spin chains,” *Phys. Rev. A* **71**, 060305 (2005).
- [108] Román Orús, “Universal geometric entanglement close to quantum phase transitions,” *Phys. Rev. Lett.* **100**, 130502 (2008).
- [109] Anindya Biswas, R. Prabhu, Aditi Sen(De), and Ujjwal Sen, “Genuine-multipartite-entanglement trends in gapless-to-gapped transitions of quantum spin systems,” *Phys. Rev. A* **90**, 032301 (2014).
- [110] Artur K. Ekert, “Quantum cryptography based on bell’s theorem,” *Phys. Rev. Lett.* **67**, 661–663 (1991).
- [111] Charles H. Bennett, Herbert J. Bernstein, Sandu Popescu, and Benjamin Schumacher, “Concentrating partial entanglement by local operations,” *Phys. Rev. A* **53**, 2046–2052 (1996).
- [112] Valerie Coffman, Joydip Kundu, and William K. Wootters, “Distributed entanglement,” *Phys. Rev. A* **61**, 052306 (2000).
- [113] B. M. Terhal, “Is entanglement monogamous?” *IBM Journal of Research and Development* **48**, 71–78 (2004).
- [114] Jeong San Kim, Gilad Gour, and Barry C. Sanders, “Limitations to sharing entanglement,” *Contemporary Physics* **53**, 417–432 (2012).
- [115] Manabendra N. Bera, R. Prabhu, Aditi Sen(De), and Ujjwal Sen, “Characterization of tripartite quantum states with vanishing monogamy score,” *Phys. Rev. A* **86**, 012319 (2012).
- [116] K. Rama Koteswara Rao, Hemant Katiyar, T. S. Mahesh, Aditi Sen (De), Ujjwal Sen, and Anil Kumar, “Multipartite quantum correlations reveal frustration in a quantum ising spin system,” *Phys. Rev. A* **88**, 022312 (2013).
- [117] Himadri Shekhar Dhar, Amit Kumar Pal, Debraj Rakshit, Aditi Sen(De), and Ujjwal Sen, “Monogamy of quantum correlations - a review,” in *Lectures on General Quantum Correlations and their Applications*, edited by Felipe Fernandes Fanchini, Diogo de Oliveira Soares Pinto, and Gerardo Adesso (Springer International Publishing, Cham, 2017) pp. 23–64.
- [118] Asher Peres, “Separability criterion for density matrices,” *Phys. Rev. Lett.* **77**, 1413–1415 (1996).
- [119] Michał Horodecki, Paweł Horodecki, and Ryszard Horodecki, “Separability of mixed states: necessary and sufficient conditions,” *Phys. Lett. A* **223**, 1–8 (1996).
- [120] Karol Życzkowski, Paweł Horodecki, Anna Sanpera, and Maciej Lewenstein, “Volume of the set of separable states,” *Phys. Rev. A* **58**, 883–892 (1998).
- [121] G. Vidal and R. F. Werner, “Computable measure of entanglement,” *Phys. Rev. A* **65**, 032314 (2002).
- [122] Jinhyoung Lee, M. S. Kim, Y. J. Park, and S. Lee, “Partial teleportation of entanglement in a noisy environment,” *Journal of Modern Optics* **47**, 2151–2164 (2000).
- [123] M. B. Plenio, “Logarithmic negativity: A full entanglement monotone that is not convex,” *Phys. Rev. Lett.* **95**, 090503 (2005).
- [124] Bruno Leggio, Anna Napoli, Hiromichi Nakazato, and Antonino Messina, “Bounds on mixed state entanglement,” *Entropy* **22** (2020), 10.3390/e22010062.
- [125] D. P. DiVincenzo, C. A. Fuchs, H. Mabuchi, J. A. Smolin, A. Thapliyal, and A. Uhlmann, “Entanglement of assistance,” *arXiv:quant-ph/9803033* (1998).

- [126] F. Verstraete, M. Popp, and J. I. Cirac, “Entanglement versus correlations in spin systems,” *Phys. Rev. Lett.* **92**, 027901 (2004).
- [127] F. Verstraete, M. A. Martín-Delgado, and J. I. Cirac, “Diverging entanglement length in gapped quantum spin systems,” *Phys. Rev. Lett.* **92**, 087201 (2004).
- [128] M. Popp, F. Verstraete, M. A. Martín-Delgado, and J. I. Cirac, “Localizable entanglement,” *Phys. Rev. A* **71**, 042306 (2005).
- [129] Debasis Sadhukhan, Sudipto Singha Roy, Amit Kumar Pal, Debraj Rakshit, Aditi Sen(De), and Ujjwal Sen, “Multipartite entanglement accumulation in quantum states: Localizable generalized geometric measure,” *Phys. Rev. A* **95**, 022301 (2017).
- [130] J Almeida, M A Martin-Delgado, and G Sierra, “Twisted-order parameter applied to dimerized ladders,” *Journal of Physics A: Mathematical and Theoretical* **41**, 485301 (2008).
- [131] J. Almeida, M. A. Martin-Delgado, and G. Sierra, “Critical lines and massive phases in quantum spin ladders with dimerization,” *Phys. Rev. B* **77**, 094415 (2008).
- [132] Philipp Krammer, Hermann Kampermann, Dagmar Bruß, Reinhold A. Bertlmann, Leong Chuang Kwek, and Chiara Macchiavello, “Multipartite entanglement detection via structure factors,” *Phys. Rev. Lett.* **103**, 100502 (2009).
- [133] A. Scheie, Pontus Laurell, A. M. Samarakoon, B. Lake, S. E. Nagler, G. E. Granroth, S. Okamoto, G. Alvarez, and D. A. Tennant, “Witnessing entanglement in quantum magnets using neutron scattering,” *Phys. Rev. B* **103**, 224434 (2021).
- [134] Harold Ollivier and Wojciech H. Zurek, “Quantum discord: A measure of the quantumness of correlations,” *Phys. Rev. Lett.* **88**, 017901 (2001).
- [135] L Henderson and V Vedral, “Classical, quantum and total correlations,” *Journal of Physics A: Mathematical and General* **34**, 6899 (2001).
- [136] Jonathan Oppenheim, Michał Horodecki, Paweł Horodecki, and Ryszard Horodecki, “Thermodynamical approach to quantifying quantum correlations,” *Phys. Rev. Lett.* **89**, 180402 (2002).
- [137] Michał Horodecki, Paweł Horodecki, Ryszard Horodecki, Jonathan Oppenheim, Aditi Sen(De), Ujjwal Sen, and Barbara Synak-Radtke, “Local versus nonlocal information in quantum-information theory: Formalism and phenomena,” *Phys. Rev. A* **71**, 062307 (2005).